MODELLING NATURAL SOILS USING STRUCTURED CAM CLAY

John P. Carter [1]
Martin D. Liu [2]
Suksun Horpibulsuk [3]

[1]Faculty of Engineering and Built Environment, University of Newcastle, NSW 2308, Australia,
John.Carter@newcastle.edu.au
[2]Faculty of Engineering, University of Wollongong, NSW 2522, Australia, martindl@uow.edu.au
[3]School of Civil Engineering, and Construction Technology Research Unit, Suranaree University of Technology,
Nakhon Ratichasima 30000, Thailand, suksun@g.sut.ac.th

ABSTRACT : A simple predictive model, referred to as Structured Cam Clay (SCC), was proposed recently by the authors. SCC was formulated for representing the mechanical behaviour of natural soils. In this paper, the main concepts and the formulation of the SCC are described and an extension of SCC for predicting the behaviour of artificially cemented clays is also presented. SCC is then used to predict the behaviour of structured soils in 'single element' compression and shearing tests. It is seen that the new model provides satisfactory qualitative and quantitative modelling of many important and unique features of the behaviour of structured soils. By using this model in finite element calculations, the response of footings founded on structured soils to loading is obtained. Some guidelines are also given to identify the importance of the structural features of the soil in determining the response of the footing. The new model is shown to be a powerful tool for geotechnical practitioners engaged in engineering design.

KEYWORDS : *constitutive model, plasticity, structure of soils, Structured Cam Clay.*

1. INTRODUCTION

Most of the constitutive models used in geotechnical engineering computations were developed to describe the behaviour of soils reconstituted in the laboratory, where the soil structure is usually standardised by the sample preparation method. However, soils in situ usually possess natural structure and consequently behave differently from the same material in a reconstituted state (e.g., Burland 1990; Leroueil and Vaughan 1990; Cuccovillo and Coop 1999; Carter et al. 2000). Indeed, significant difficulties have been encountered in cases where the structural features of the soil dominate its engineering behaviour. The low driving resistance of piles observed in carbonate soils at the North Rankin offshore gas production platform, Australia (King and Lodge 1988) and the subsidence induced during hydrocarbon extraction from reservoirs at Ekofisk, North Sea (Potts et al. 1988) are but two well-known examples. For natural soils, the structure may arise from many different causes. Various geological processes as well as loading can cause a loss of soil structure either by inducing yield (damaging the bonding or permanently rearranging the particles) or by removing bonding agents. Nevertheless, the effects of soil structure on the mechanical behaviour have been shown to be similar (Gens and Nova 1993; Leroueil and Vaughan 1999; Liu and Carter 1999). It is therefore possible to unite the mechanical behaviour of various natural soils into a consistent theoretical framework.

Recently, there have been important developments in understanding the mechanics of structured soils. At a fundamental level, there have been useful advances in formulating constitutive models incorporating the influence of soil structure, such as those proposed by Gens and Nova (1993), Whittle (1993), Rouainia and Muir Wood (2000), Kavvadas and Amorosi (2000). The main objective of the formulation of the SCC model by Liu and Carter (Liu and Carter 2002; Carter and Liu 2005) was to provide a relatively simple constitutive model suitable for the solution of boundary value problems encountered in geotechnical engineering practice. The model is a rational extension of the well-known Modified Cam Clay (MCC) model and has relatively few parameters, each of which has a clear physical meaning and can be conveniently identified. SCC has also been used to predict the behaviour of a variety of structured natural soils in both compression and shearing tests. It has been demonstrated that the SCC model captures well the main features of the behaviour of natural clays in both single element tests and boundary value problems, under both drained and undrained conditions.

This paper contains the following four parts: (1) a summary of the concepts and formulation of the Structured Cam Clay model; (2) the extension of the model for artificially cemented clays; (3) investigation of the capacity of the model for describing laboratory single element tests; and (4) a description of the capability of the model for solving boundary value problems.

The stress and strain quantities used to describe soil behaviour are defined in the following section. The properties of a reconstituted soil are called the intrinsic properties, and are denoted by the symbol * attached to the relevant symbols.
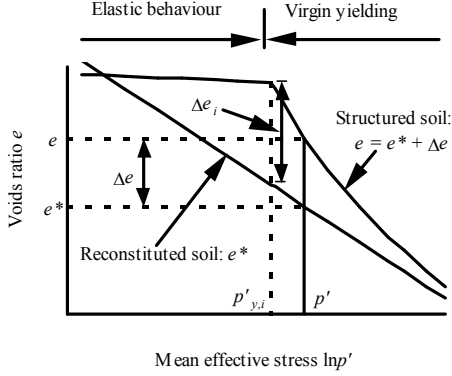
Figure 1 Material idealisation

2. STRESS AND STRAIN PARAMETERS

The stress and strain quantities used in the model formulation are defined as follows. The mean effective stress is given by

$$p' = \frac{1}{3}\left(\sigma'_{11} + \sigma'_{22} + \sigma'_{33}\right)$$
$$= \frac{1}{3}\left(\sigma'_1 + 2\sigma'_2\right) \text{(for conventional triaxial tests)} \tag{1}$$

and the deviatoric stress by

$$q = \frac{1}{\sqrt{2}} \sqrt{\begin{bmatrix} \left(\sigma'_{11} - \sigma'_{22}\right)^2 + \left(\sigma'_{22} - \sigma'_{33}\right)^2 + \\ \left(\sigma'_{33} - \sigma'_{11}\right)^2 + \\ 6\left(\sigma'_{12}{}^2 + \sigma'_{23}{}^2 + \sigma'_{31}{}^2\right) \end{bmatrix}}$$
$$= \left(\sigma'_1 - \sigma'_2\right) \text{(for conventional triaxial tests)} \tag{2}$$

in which σ'_{ij} are the Cartesian components of an effective stress state.

The stress ratio η is defined as

$$\eta = \frac{q}{p'} \tag{3}$$

The corresponding incremental volumetric and deviatoric strains are defined as

$$d\varepsilon_v = d\varepsilon_{11} + d\varepsilon_{22} + d\varepsilon_{33}$$
$$= d\varepsilon_1 + 2d\varepsilon_2 \text{ (for conventional triaxial tests)} \tag{4}$$

and

$$d\varepsilon_d = \frac{\sqrt{2}}{3} \sqrt{\begin{bmatrix} \left(d\varepsilon_{11} - d\varepsilon_{22}\right)^2 + \left(d\varepsilon_{22} - d\varepsilon_{33}\right)^2 + \\ \left(d\varepsilon_{33} - d\varepsilon_{11}\right)^2 + \\ 6\left(d\varepsilon_{12}{}^2 + d\varepsilon_{23}{}^2 + d\varepsilon_{31}{}^2\right) \end{bmatrix}}$$
$$= \frac{2}{3}\left(d\varepsilon_1 - d\varepsilon_2\right) \text{(for conventional triaxial tests)} \tag{5}$$

3. FORMULATION OF THE STRUCTURED CAM CLAY MODEL

In the formulation of the Structured Cam Clay model, it is assumed that the behaviour of soil in a reconstituted state can be described adequately by the Modified Cam Clay model (Roscoe and Burland 1968), which is employed as a basis for formulating the Structured Cam Clay model.

The formation and development of soil structure often produces soil anisotropy. Destructuring usually leads to the reduction of anisotropy. However, for simplicity, only the isotropic variation of the mechanical properties associated with soil structure is described in this theoretical framework.

3.1 Influence of soil structure on isotropic virgin compression

Research on the compression behaviour of soils by Liu and Carter (1999 and 2000a) is employed here as a starting point for including the effects of soil structure in the model. The material idealisation of the isotropic compression behaviour of structured clay is illustrated in Figure 1. In this figure e represents the voids ratio for a structured clay, $e*$ is the voids ratio for the corresponding reconstituted soil at the same stress state during virgin yielding, $p'_{y,i}$ is the mean effective stress at which virgin yielding of the structured soil begins, and Δe, the additional voids ratio sustained by soil structure, is the difference in voids ratio between a structured soil and the corresponding reconstituted soil at the same stress state. Hence, the isotropic virgin compression behaviour of a structured soil can be expressed simply as

$$e = e* + \Delta e \tag{6}$$

A general form of the equation describing the additional voids ratio during the isotropic virgin compression of natural clays was proposed as (Liu and Carter 1999, 2000a)

$$\Delta e = a\left(\frac{p'_{y,i}}{p'}\right)^b + c \tag{7}$$

where b is a parameter quantifying the rate of destructuring, termed the *destructuring index*, and c is that part of the additional voids ratio sustained by structure that cannot be eliminated by an increase in stress. Parameters a, b and c satisfy the following condition

$$c = \lim_{p' \to \infty} \Delta e \tag{8}$$

and

$$a = \Delta e_i - c \tag{9}$$

where Δe_i is the initial additional voids ratio at $p' = p'_{y,i}$, where virgin yielding of the structured soil begins (Figure 1). Residual additional voids ratio c is associated with meta-stable structure of soil, which normally will not be altered by loading. A detailed study of the behaviour of soil with meta-stable structure can be found in the paper by Cotecchia and Chandler (1997).

3.2 Yield surface for structured clay

In the proposed model, the behaviour of clay is divided into virgin yielding behaviour and elastic behaviour by its current yield surface, i.e., the structural yield surface, which is defined by the current stress state, voids ratio, stress history, and soil structure. Similar to the original proposal by Roscoe and Burland (1968), the yield surface of a structured soil in p'-q space is assumed to be elliptical in the first instance and to pass through the origin of the stress coordinates (Figure 2). The aspect ratio for the structural yield surface is M*, the critical state stress ratio of the reconstituted soil. p'_s, the value of the p' coordinate where the ellipse again intersects the axis, represents the size of the structural yield surface. The yield surface is thus given by the yield function f, where

$$f = q^2 - M^{*2} p'(p'_s - p') = 0 \quad (10)$$
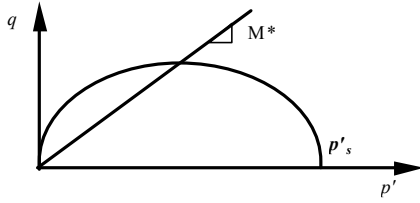
Figure 2 Yield surface for soils

3.3 Virgin yielding along general stress paths

According to Critical State Soil Mechanics (Schofield and Wroth 1968), both virgin yielding and elastic compression behaviour of reconstituted clay are linear in e - $\ln p'$ space, with gradients $\lambda*$ and $\kappa*$ respectively. Thus, isotropic virgin compression line for the reconstituted soil is given by

$$e* = e*_{IC} - \lambda* \ln p' \quad (11)$$

where $e*_{IC}$ is the voids ratio of the reconstituted soil when p' = 1 kPa during virgin isotropic compression.

We seek now to generalise equation (11) for a soil that possesses structure. There are two basic assumptions in the derivation. The first one is that both the hardening and the destructuring of natural clay are dependent on plastic volumetric deformation. The second is that the elastic properties of a soil are independent of soil structure.

On substituting equations (11) and (7) into equation (6), the following expression for the variation of the voids ratio is obtained

$$e = e*_{IC} + a\left(\frac{p'_{y,i}}{p'}\right)^b + c - \lambda* \ln p' \quad (12)$$

According to Critical State Soil Mechanics, for loading along a general stress path the volumetric deformation of a reconstituted soil, defined by $\lambda* \ln p'$ in the above equation, can be divided into two parts. The elastic part is defined by $\kappa* \ln p'$, which is dependent on the current mean effective stress. The plastic part is

given by $(\lambda*-\kappa*)\ln p'_s$, which is dependent on the size of the yield surface. Thus equation (12) can be rewritten as

$$e = e*_{IC} - \kappa* \ln p' + a\left(\frac{p'_{y,i}}{p'}\right) - (\lambda*-\kappa*)\ln p'_s + c \quad (13)$$

Based on the volumetric-dependent hardening and destructuring assumption, the plastic part of the voids ratio change is dependent on the size of the current yield surface, not the mean effective stress or shear stress (a comprehensive study of the volumetric dependent hardening of reconstituted and naturally structured clays can be found in papers by Liu and Carter 2000b and 2003). Because the elastic properties of soil are assumed to be independent of soil structure, the deformation associated with the additional voids ratio sustained by soil structure is plastic. Hence p' in the third term of equation (13) should also be substituted by the size of the current structural yield surface, p'_s. As can be seen from equation (10), for isotropic compression the size of the yield surface is equal to the value of the current mean effective stress, therefore equation (13) can be rewritten as

$$e = e*_{IC} - \kappa* \ln p' + a\left(\frac{p'_{y,i}}{p'_s}\right) - (\lambda*-\kappa*)\ln p'_s + c \quad (14)$$

Equation (14) describes the change of voids ratio and it contains three basic terms that vary with stress state. It is valid for loading along general stress paths. Taking the differential form of equation (14) and dividing both sides by $(1+e)$, the following equation for the total volumetric strain increment is obtained

$$d\varepsilon_v = \frac{\kappa*}{1+e}\left(\frac{dp'}{p'}\right) + \left[(\lambda*-\kappa*) + b\langle\Delta e - c\rangle\right]\frac{dp'_s}{(1+e)p'_s} \quad (15)$$

where

$$\langle a \rangle = \begin{cases} a \text{ if } a \geq 0 \\ 0 \text{ if } a < 0 \end{cases} \quad (16)$$

Δe is the current value of the additional voids ratio sustained by soil structure for loading along general stress paths. It is necessary to add the sign function $\langle\rangle$ to the term $(\Delta e - c)$ in equation (15) because, as noted previously, the voids ratio component c cannot be reduced by an increase in compressive stress.

The first part of equation (15) represents elastic deformation, and the second part represents the plastic deformation. If the effect of shearing on destructuring is also considered, a modification to the derived volumetric strain increment is required and the final equation proposed for the SCC model is as follows

$$d\varepsilon_v = \frac{\kappa* dp'}{(1+e)p'} + (\lambda*-\kappa*)\frac{dp'_s}{(1+e)p'_s} + \left[\langle\Delta e - c\rangle + \frac{\gamma\eta\Delta e}{M*-\eta}\right]\frac{bdp'_s}{(1+e)p'_s} \quad (17)$$

where γ is a model parameter. It is seen from the above equation that the effect of shearing on destructuring is directly proportional to the value of γ.

The plastic strain increment $d\varepsilon^p_v$ can therefore be expressed as

$$d\varepsilon^p_v = \left(\lambda* - \kappa*\right)\frac{dp'_s}{\left(1+e\right)p'_s}$$
$$+\left[\langle\Delta e - c\rangle + \frac{\gamma\eta\Delta e}{M*-\eta}\right]\frac{bdp'_s}{\left(1+e\right)p'_s} \qquad (18)$$

The plastic volumetric deformation is made up of two parts, viz., the part associated with the intrinsic properties of the soil and that associated with soil structure.

3.4 Deviatoric deformation for virgin yielding

The structure of soil also has an influence on the flow rule. It is observed that a structured clay with positive Δe generally has a lower value for the strain increment ratio $d\varepsilon^p_d/d\varepsilon^p_v$ than the corresponding reconstituted soil at the same virgin yielding stress state (e.g., Graham and Li 1985; Cotecchia and Chandler 1997). Based on a trial and error method, one form of the new flow rule is proposed for naturally structured clays as

$$\frac{d\varepsilon^p_d}{d\varepsilon^p_v} = \frac{2\eta}{\left|M*^2 - \eta^2\right| + \omega\eta^2\left|1 - \sqrt{p'_e/p'_s}\right|} \qquad (19)$$

where ω is a model parameter, $|x|$ represents the absolute value of the quantity x, and p'_e is the size of the equivalent yield surface for a structured soil, which is defined as the yield surface for the same soil in a reference state with the same voids ratio and the same stress state. The size of the equivalent yield surface, denoted by p'_e, is given by

$$p'_e = \frac{e^{\left(\frac{e_{IC}* - e + c}{\lambda* - \kappa*}\right)}}{p'^{\left(\frac{\kappa*}{\lambda*-\kappa*}\right)}} \qquad (20)$$

As can be seen from the above equation, this reference state is different from a reconstituted state for soils with $c \neq 0$.

The deviatoric strain increment during virgin yielding is thus obtained as

$$d\varepsilon_v = d\varepsilon^e_d + \frac{2\eta}{\left|M*^2-\eta^2\right| + \omega\eta^2\left|1-\sqrt{p'_e/p'_s}\right|} \times$$
$$\left\{\left(\lambda*-\kappa*\right) + b\left[\langle\Delta e - c\rangle + \frac{\gamma\eta\Delta e}{M*-\eta}\right]\right\}\frac{dp'_s}{\left(1+e\right)p'_s} \qquad (21)$$

3.5 Elastic behaviour

For stress excursions within the current virgin yielding boundary, only elastic deformation occurs. The elastic deformation of a structured soil is assumed to follow Hooke's law, and to be independent of soil structure. The elastic deformation can be written as

$$d\varepsilon^e_v = \frac{3\left(1-2\nu*\right)}{E*}dp' \qquad (22)$$

$$d\varepsilon^e_d = \frac{2\left(1+\nu*\right)}{3}\frac{dq}{E*} \qquad (23)$$

where $\nu*$ is Poisson's ratio and $E*$ is the Young's modulus. $E*$, $\nu*$, p', and the elastic swelling index $\kappa*$ are related by

$$E* = \frac{3\left(1-2\nu*\right)\left(1+e\right)}{\kappa*}p' \qquad (24)$$

The adoption of equations (22), (23) and (24) to describe elastic deformation allows the selection of either constant swelling index $\kappa*$ or constant Young's modulus $E*$. The selection of constant $E*$ indicates a linear $e - p'$ relationship for elastic deformation, as observed for some natural clays (e.g., Wong 1980; Lagioia and Nova 1995; Carter et al. 2000). For this selection, the reduction in voids ratio associated with plastic deformation of reconstituted clay is no longer linear in the $e - \ln p'_s$ space, and neither is the critical state line. Consequently, equations such as those given by (11), (17) and (21) represent only an approximation of actual soil behaviour by assuming a linear $e - \ln p'_s$ relationship for plastic deformation of soil in reconstituted states.

A constraint on the value of the elastic deformation parameter $\kappa*$ is proposed so that the Young's modulus $E*$ will not be infinitesimal as p' approaches zero, i.e.,

$$\kappa* \leq 3\left(\frac{p'}{p'_s}\right)\lambda* \qquad (25)$$

The adoption of this constraint avoids numerical problems. For example, the softening behaviour of highly overconsolidated soil can thus be predicted, because the situation where elastic deformation is much larger than the corresponding plastic deformation during softening is avoided.

3.6 Softening and crushing of soil structure

For stress states on the yield surface and with $\eta > M*$, softening occurs. As is the situation for most models of the Cam Clay family, during a softening process, soil behaves as a virgin yielding material and the stress state remains on the yield surface. As previously suggested (Liu and Carter 2002), the volumetric deformation of a structured clay during softening is described by the same equation as for virgin yielding, i.e., equation (17). However, the sign of the plastic deviatoric strain associated with destructuring has to be changed, so that the strain increment vector will always point outside the yield surface, i.e.,

$$d\varepsilon^p_d = \frac{-2\eta}{\left|M*^2-\eta^2\right| + \omega\eta^2\left|1-\sqrt{p'_e/p'_s}\right|}\frac{dp'_s}{\left(1+e\right)p'_s} \times$$
$$\left\{\left(\lambda^*-\kappa^*\right) + b\left[\langle\Delta e - c\rangle - \frac{\gamma\eta\Delta e}{M*-\eta}\right]\right\} \qquad (26)$$

It may be noticed that for both virgin yielding and softening behaviour, the soil may reach a state with $\eta = M*$ but with $\Delta e \neq 0$. As is indicated in the flow rule,

i.e., equation (19), in such cases the resistance of the soil to continuous shear deformation is not zero. Clearly, the critical state of deformation has not been achieved at this stage, even though the stress state has reached the Critical State Line (CSL) in p' - q space. In a continuing shearing test, the soil will experience a transition from its current state to the critical state of deformation. During the transition to the critical state of deformation, soil experiences re-arrangement of its structure and plastic deformation will be produced. It is assumed that during the process of the crushing of structure, soil behaves as a virgin yielding material and that the stress state remains on the yield surface. It is also assumed that during this transition the effective stress state of the soil always stays on the CSL but may travel along the line either upwards or downwards, i.e., hardening or softening.

The stress and strain relationship for this transition process is described by the following set of equations

$$
\begin{cases}
dq = \mathrm{M}^* dp' \\
dp' \geq 0 \text{ for } p'_s < p'_e, \text{ and } dp' \leq 0 \text{ for } p'_s > p'_e \\
d\varepsilon_v = \left(\dfrac{\kappa^*}{1+e}\right)\dfrac{dp'}{p'} + d\varepsilon_v^p \\
d\varepsilon_d = \dfrac{2(1+\nu^*)}{9(1-2\nu^*)}\left(\dfrac{\kappa^*}{1+e}\right)\dfrac{dq}{p'} + \dfrac{2\left|d\varepsilon_v^p\right|}{\omega\eta\left|1-\sqrt{p'_e/p'_s}\right|}
\end{cases}
\tag{27}
$$

There are now three equations for the three unknown quantities: dp', dq and $d\varepsilon_v^p$, and consequently the stress strain relationship for the critical state transition is fully defined. During this process of structural adjustment, the additional voids ratio of the soil continues to decrease until it reaches the residual additional voids ratio c, and at the end of the process the soil reaches a critical state of deformation, irrespective of its original structure.

3.7 Modification of the virgin yielding locus

In order to model accurately the influence of the initial soil structure on the virgin yielding boundary, a simple modification is proposed, so that the initial structural yield surface is allowed to possess a shape different from the elliptical yield surface associated with stress history. The modification is relatively straightforward and involves extension of the concept of virgin yielding.

Suppose that the initial structural yield surface may be expressed as

$$f_{s,i}(p', q) = 0 \tag{28}$$

Suppose the initial state of a soil be denoted as point A and the soil is loaded along stress path AB (Figure 3). When the current stress state reaches the initial structural yield surface $f_{s,i}$ at point C, virgin yielding occurs. For continuing loading, the virgin yielding boundary is made of the two areas defined by the initial structural yield surface $f_{s,i}$ and $p'_{c,max}$. $p'_{c,max}$ is the maximum size of the stress yield surface the soil has ever experienced, which is defined by equation (10). The value of $p'_{c,max}$

corresponding to stress state B for stress path AB is shown in Figure 3. If the stress state of the soil turns inside the current yielding boundary, the soil behaves as a purely elastic material, and the boundary remains unchanged.
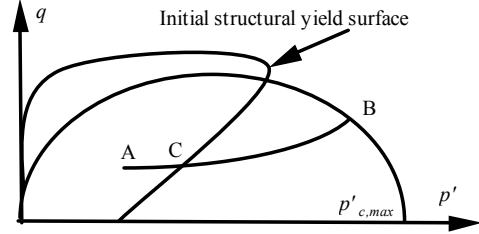
Figure 3 Virgin yielding boundary

The virgin yielding boundary is described by $p'_{c,max}$ completely when the initial structural yield surface $f_{s,i}$ is contained within the surface defined by $p'_{c,max}$. After that the initial structural yield surface no longer has any influence on the soil behaviour. It is also assumed that the moment softening occurs the initial structural yield surface is destroyed. The current yield surface is identical to the virgin yielding boundary.

Table 1 Properties of Structured Cam Clay

Symbol	Description
Reconstituted soil properties	
λ^*	gradient of the normal compression line in e-$\ln p'$ space
κ^*	gradient of the unloading and reloading line in e-$\ln p'$ space
M^*	critical state stress ratio
ν^*	Poisson's ratio
e^*_{cs}	void ratio at the $p' = 1$ on the CSL in e-$\ln p'$ space
Additional parameters defining soil structure	
b	destructuring index
Δe_i	additional voids ratio sustained by soil structure ($= a + c$)
c	additional voids ratio sustained by soil structure at very large confining pressures
$p'_{y,i}$	size of the initial (structural) yield surface
γ	parameter defining the plastic potential
ω	flow rule parameter

It is obvious that the concept of yielding introduced above is valid no matter if the initial structural yield surface and the elliptical yield surface associated with loading are identical or not.

3.7 Model parameters

Ten parameters define the Structured Cam Clay model, and they are M*, e^*_{IC}, λ^*, κ^*, ν^*, b, c, γ, ω and $p'_{y,i}$ (or the initial structural yield surface $f_{s,i}$), as listed in Table 1.

The first five parameters, denoted by the symbol *, are intrinsic soil properties. They are independent of soil structure. These five intrinsic parameters are the same as those adopted in the Modified Cam Clay model (e.g., Muir Wood 1990).

The new parameters, viz., b, c, γ, ω and $p'_{y,i}$ (or $f_{s,i}$) are introduced to describe the influence of soil structure on its mechanical behaviour. A detailed study of parameters b and $p'_{y,i}$ on the compression behaviour of natural clays can be found in the paper by Liu and Carter (2000a). Parameter c is a measure of the ultimate separation of the isotropic compression line for a structured soil and the same soil in a reconstituted state. It can be seen that these three parameters have clear physical meaning, and can be determined conveniently from an isotropic compression test or an oedometer test on an intact soil sample.

Parameter γ describes the reduction of the additional voids ratio sustained by soil structure associated with current shear stress. The total plastic volumetric deformation associated with the additional voids ratio is described completely in terms of four material parameters, i.e., M*, b, c and γ. The first three parameters can be determined independently from experimental data. Consequently, parameter γ can be identified independently by studying the variation of Δe with η under virgin shearing. Parameter ω describes the flow rule and can be determined from the measured plastic strain increment vector. Theoretically, all the five new parameters can be identified directly from conventional tests on structured clays.

The adoption of an initial structural yield surface $f_{s,i}$ different from that described by yield surface function (10) is suggested if there is enough experimental evidence to justify such a choice. A detailed study on identifying the initial structural yield surface $f_{s,i}$ can be found in a paper by Diaz-Rodriguez et al. (1992).

4. EXTENSION OF SCC FOR CEMENTED CLAYS

As previously stated, the major aim of formulating the Structured Cam Clay model was to provide a constitutive model suitable for the solution of boundary value problems encountered in geotechnical engineering practice, i.e., a practical tool. It was therefore necessary to keep the model relatively simple. It is perceived that a simple predictive model should possess the following features: overall a simple and consistent physical basis for the model, an explicitly expressed D matrix, and model parameters with clear physical meanings and which are identifiable from conventional laboratory tests. Following this principle, a simple and straightforward modification of the model is made so that the influence of cementation is incorporated into the model directly.

4.1 Mechanical properties of cemented clays

Based on a large body of experimental data (e.g., Huang and Airey 1998; Ismail et al. 2002; Rotta et al. 2003; Horpibulsuk, 2001; Horpibulsuk et al. 2004a and b,

2005), the following characteristics of cemented clays are observed.

(1) From comparison of the behaviour of clay in reconstituted states, naturally structured states and cemented states, it is seen that the basic behaviour of an artificially cemented clay is similar to that of a naturally structured clay (Airey 1990; Liu and Carter 1999; Carter et al. 2000). The voids ratio sustained by an artificially cemented clay is higher than that of the same soil without cementation. During yielding, destructuring takes place. However, the voids ratio sustained by cementation structure is usually much higher than that sustained by natural structure, but the rate of destructuring is considerably lower than that of naturally structured clays.

(2) The size of the initial yield surface increases with cementation and so does the tensile strength of the soil. Also, the elastic region inside the yield surface increases with cementation.

(3) The final strength of cemented clay, both in terms of shear stress and stress ratio, is generally higher than that of the same soil without cementation. The final shear stress ratio is also improved. However, the change in the final stress ratio is insignificant with cement content, provided that the content is above a critical value. The final shear stress and mean effective stress of an artificially cemented clay are generally much higher than those of the same soil without cementation. This feature is fundamentally different from that of a naturally structured clay (Burland 1990). Nevertheless, the behaviour of cemented soil is essentially that of a frictional material.

Based on both qualitative and quantitative observation, two simple and direct modifications are proposed to take into consideration the influence of cementation on soil behaviour. They are a modification to the mean effective stress parameter and the modelling of the breakdown of cementation.

4.2 Modified mean effective stress parameter

Based on the analysis of experimental data (Horpibulsuk 2004b; Kasama et al. 2000), it is concluded that the behaviour of cemented clays principally follows rules of cohesionless soils provided the effect of cementation is taken into consideration as a boost to the mean effective stress. Therefore, a modified mean stress parameter is proposed as follows

$$\bar{p}' = p' + C/_{M^*} \qquad (29)$$

where M* is the critical state strength of the soil, and C is a parameter related to the shear strength contributed by cementation. The stress ratio is modified accordingly

$$\bar{\eta} = \frac{q}{\bar{p}'} \qquad (30)$$

4.3 Breakdown of cementation

For simplicity, the breakdown of the cementation, i.e., the crushing of soil structure, is assumed to occur as the soil approaches the final critical state of deformation. As

discussed in section 3.6, during crushing of the structure the stress state stays on the critical state line. By a process of trial and error it has been suggested that the function describing the breakdown of cementation should be

$$dC = -2\left(\frac{C}{C_{in}}\right)\frac{|dp'|}{\sqrt{\left(\frac{q}{p'}-\mathrm{M}^*\right)}} \qquad (31)$$

where C_{in} is the value of the initial cementation strength.

The general stress and strain relationships describing this process are proposed as

$$\begin{cases} dq = \mathrm{M}^* dp' - dC \\ d\varepsilon_v = \left(\dfrac{\kappa}{1+e}\right)\dfrac{dp'}{\bar{p}'} + d\varepsilon_v^p \\ d\varepsilon_d = \dfrac{2(1+\nu)}{9(1-2\nu)}\left(\dfrac{\kappa}{1+e}\right)\dfrac{dq}{p'} + \dfrac{2\bar{\eta}\left|d\varepsilon_v^p\right|}{\omega(1-2\nu)\left|1-\sqrt{p_o'/p_s'}\right|} \end{cases} \qquad (32)$$

For cemented soils the following compression equation is proposed

$$e = e^* + (\Delta e_i - c)\left(\frac{p_{y,i}' + C/\mathrm{M}^*}{\bar{p}'}\right) + c \qquad (33)$$

and the yield surface is now given by

$$f = q^2 - \mathrm{M}^* \bar{p}'(p_s' - \bar{p}') = 0 \qquad (34)$$

where p_s' is the size of the yield surface. As illustrated in Figure 4, the yield surface for the cemented soil is effectively shifted to the left along the p' axis by a distance of C/M^*.

Figure 4 Yield surfaces

In the model for cemented soil, the slope of the crushing envelope and the critical state line are assumed to be the same (Wissa et al. 1965; Clough et al. 1981; Kasama et al. 2000) and equal to M*. The size of the initial yield surface, $p_{s,i}'$, is linked to the initial mean effective yield stress, $p_{y,i}'$, by the following equation

$$p_{s,i}' = p_{y,i}' + C/\mathrm{M}^* \qquad (35)$$

4.4 Strain relationships

With the modifications introduced to describe the effect of cementation, the following incremental stress and strain relationship for a cemented clay during virgin yielding can be obtained

$$\begin{cases} d\varepsilon_v = d\varepsilon_v^e + \left\{(\lambda^*-\kappa) + b\langle\Delta e - c\rangle\left[1+\dfrac{\gamma\bar{\eta}}{\mathrm{M}^*-\bar{\eta}}\right]\right\}\dfrac{dp_s'}{(1+e)p_s'} \\ d\varepsilon_d = d\varepsilon_d^e + \dfrac{2\bar{\eta}}{\left|\mathrm{M}^{*2}-\bar{\eta}^2\right| + \omega\left|1-\sqrt{p_o'/p_s'}\right|} \times \\ \qquad \left\{(\lambda^*-\kappa) + b\langle\Delta e - c\rangle\left[1+\dfrac{\gamma\bar{\eta}}{\mathrm{M}^*-\bar{\eta}}\right]\right\}\dfrac{dp_s'}{(1+e)p_s'} \end{cases} \qquad (36)$$

5. MODEL EVALUATION

The validity of the Structured Cam Clay model and its generalization for cemented clays is investigated in this section by comparing the predictions of these models with some of the available data obtained from single element tests on structured soils.

5.1 Compression behaviour of two clays

Two sets of compression tests on different soils were simulated and for these tests only the volumetric deformation has been computed. As can be seen from equation (17), the volumetric deformation is not influenced by the values of parameters ν^* and ω. Hence, for the present purpose there is no need to determine or specify values for these parameters.

5.1.1 Leda clay

The first group of test data includes five compression tests on natural soft Leda clay performed by Yong and Nagaraj (1977) and Walker and Raymond (1969). The two oedometer tests on the natural and reconstituted Leda clay reported by Yong and Nagaraj (1977) were used to identify soil parameters, and their values are listed in Table 2. The initial state of the structured soil is defined by $\sigma'_v = 20$ kPa and $e = 1.96$. As shown in Figure 5, the compression behaviour of Leda clay is well simulated by the model.

Figure 5 Behaviour of Leda clay in an oedometer test (Test data after Yong ang Nagaraj 1977)

Three tests performed by Walker and Raymond (1969) were used to evaluate the model's predictions. Although all the specimens tested by both Yong and

Nagaraji (1977) and Walker and Raymond (1969) were Leda clay, they were obtained from different locations in the same area. It is assumed that these specimens differed only in the size of the initial yield surface, i.e., the different Leda clay samples possessed the same mineralogy and type of structure but may have had different degrees of structure. The three compression tests were with $\eta = 0$, 0.63 and 1 respectively. The experimental data for the test with $\eta = 0$ were used to identify the size of the yield surface, and it was found that $p'_{co} = 265$ kPa. It is seen in Figures 5 and 6 that the model gives an approximate but reasonable description of the compression behaviour of natural Leda clay.

Table 2 Model parameters for Leda clay

M*	λ*	κ*	e*$_{IC}$	b
1.2	0.223	0.03	2.338	1
c	γ	p'$_{y,i}$(kPa)		
0	0	168.6		
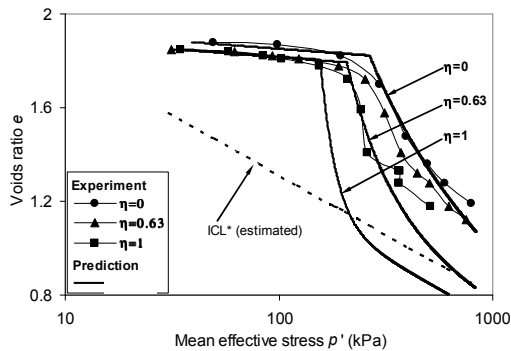
Figure 6 Compression behaviour of Leda clay (Test data after Walker and Raymond 1969)

5.1.2 Bangkok clay

The second group of test data includes the results of five compression tests on weathered Bangkok clay performed by Balasubramanian and Hwang (1980). Values of the model parameters are listed in Table 3. The one-dimensional compression curve for the reconstituted soil type was estimated by the empirical method suggested by Burland (1990), based on which parameters λ^* and e^*_{IC} were estimated. The simulated behaviour of Bangkok clay is shown in Figure 7. It may be noticed that the compression behaviour of the Bangkok clay is well simulated in this case.

The predicted compression behaviour of Bangkok clay with $\eta = 0.16$, 0.43, 0.6 and 0.75 is shown in Figure 8. These test specimens were obtained from the field and some variation in the their initial structure would normally be expected. It may be seen that the initial soil states for the five specimens may be divided into three groups, i.e., the test with $\eta = 0$, the test with $\eta = 0.16$, and tests with $\eta = 0.43$ and 0.6 and 0.75. It is assumed in the simulations that the differences in the initial states of the soil can be represented adequately by the differences in the sizes of the initial structural yield surfaces. It may be seen from the compression curve that the initial stress

state for the test with $\eta = 0.16$ is on the yield surface, i.e., $p'_{co} = 67.6$ kPa. The size of the initial yield surface for the other three specimens is 45 kPa (the test with $\eta = 0.43$ is used to identify the value of this parameter). Overall, it is seen that the proposed model gives a reasonably good approximation of the compression behaviour of weathered Bangkok clay.

Table 3 Model parameters for Bangkok clay

M*	λ*	κ*	e*$_{IC}$	b
0.9	0.4	0.1	3.82	0.5
c	γ	p'$_{y,i}$(kPa)		
0	0	35		
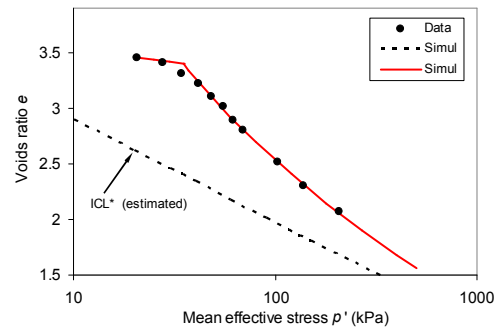
Figure 7 Compression behaviour of Bangkok clay (Test data after Balasubramanian and Hwang 1980)
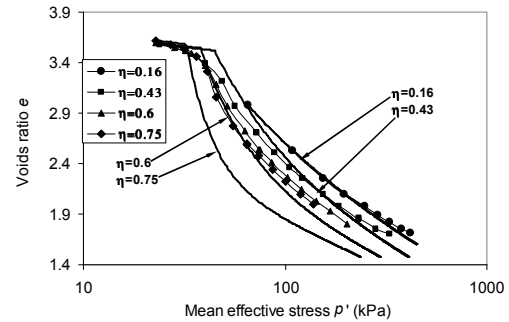
Figure 8 Compression behaviour of Bangkok clay (Test data after Balasubramanian and Hwang 1980)

5.2 Drained behaviour of natural calcarenite

Results of experimental work carried out by Lagioia and Nova (1995) on a natural calcarenite have been compared with the model predictions. The natural calcarenite was formed by marine deposition. It is a coarse-grained material with a high degree of uniformity and calcareous inter-particle cement. An isotropic compression test on the cemented soil was used to identify soil parameters and their values are listed in Table 4 (Figure 9). The value of Poisson's ratio and the critical state strength for the natural calcarenite were reported by Lagioia and Nova (1995). The initial state for the structured soil is defined by $p' = 147$ kPa and $e = 1.148$, and so the initial value of the additional voids ratio due to soil structure is $\Delta e_i = 0.15$. The value of

parameter ω was determining by curve fitting. Since E^* is assumed here to be a material constant, κ^* is calculated from equation (24). This value of κ^* is used in calculating the plastic deformation in equations (17), (21) and (25).
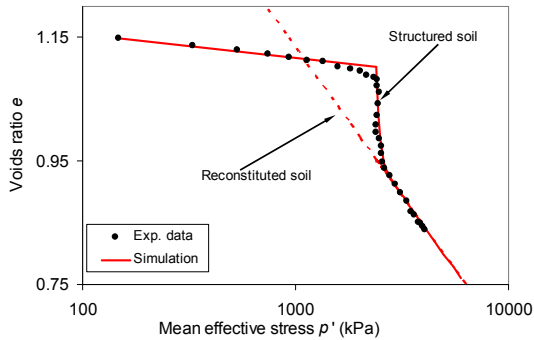
Figure 9 Isotropic compression test on a calcarenite (Test data after Lagioia and Nova 1995)

Table 4 Model parameters for a natural calcarenite

M*	λ^*	E^* (kPa)	e^*_{IC}	ν^*
1.45	0.208	76,923	2.383	0.13
b	c	ω	γ	
30	0	4	2.1	
Initial structural yield surface: ellipse with $p'_{y,i}$ = 2,400 kPa and aspect ratio = 1.12.				

In all, eight drained shearing tests were considered with the confining pressure σ'_3 ranging from 25 kPa to 3,500 kPa. A comparison between test results and the predictions for three tests are shown in Figures 10 to 12. For the test with σ'_3 = 3,500 kPa, the initial stress state is much larger than the size of the initial structural yield surface. According to the proposed model, the structure of the soil at σ'_3 = 3,500 kPa is effectively completely destroyed since the soil has a very high destructuring index, i.e., b = 30. Thus, the soil behaved essentially as a reconstituted material throughout this test. Destructuring of this sample was confirmed by Lagioia and Nova (1995).

Considering the wide range of initial stresses, it is seen that the proposed model provides successful predictions of the behaviour of this natural and highly structured calcarenite. It is also observed in the simulations and in the experimental data (Figure 11) that both the deviatoric and the volumetric strains increase virtually at constant stress at the moment when virgin yielding commences, and that a large amount of plastic deformation is accumulated at the end of this process. These simulations are consistent with experimental observations of natural soil behaviour where the soils have a very sensitive structure (e.g., Westerberg 1995, Rouainia and Muir Wood 2000; Arces et al. 1998). It is also seen that for this particular soil, the proposed material idealisation, e.g., purely elastic behaviour for loading within the current structural yield surface, represents the soil accurately (see Figures 10 and 11).

Figure 10 Shearing behaviour of a calcarenite at σ'_3 = 1300 kPa (Test data after Lagioia and Nova 1995)

Figure 11 Shearing behaviour of a calcarenite at σ'_3 = 25 kPa (Test data after Lagioia and Nova 1995)
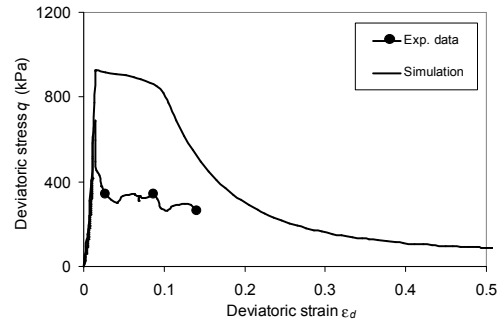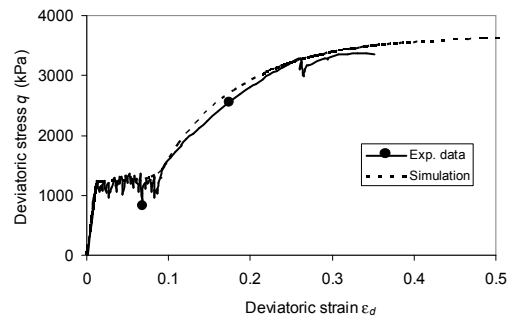
(a) Deviatoric stress and strain relationship
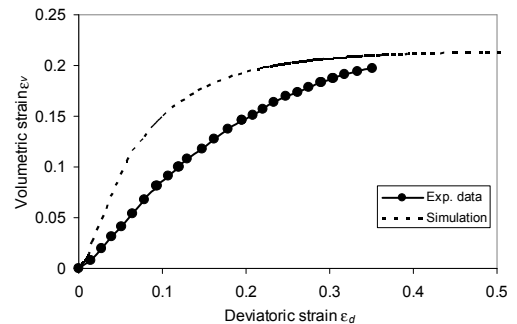
(b) Volumetric strain and deviatoric strain relationship
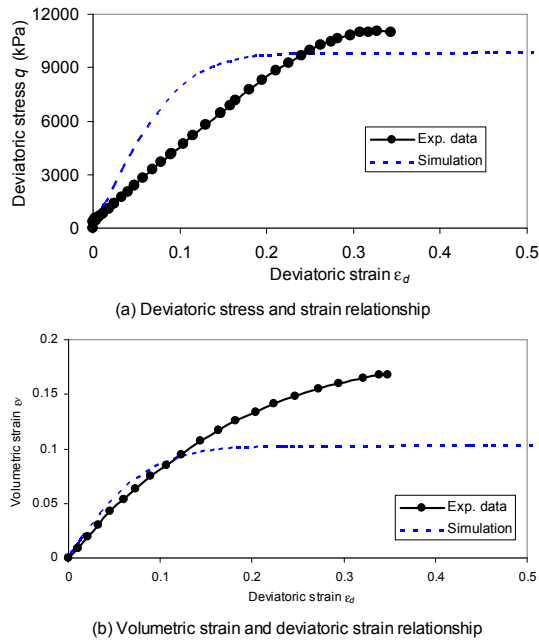
Figure 12 Shearing behaviour of a calcarenite at $\sigma'_3 = 3500$ kPa (Test data after Lagioia and Nova 1995)

5.3 Emmerstad clay

The behaviour of a natural sensitive Norwegian marine clay, Emmerstad clay, was simulated and the predictions compared with data from undrained triaxial tests performed by Lacasse et al. (1985) (from Burland 1990). Both compression and extension tests are compared. In all tests, intact soil specimens were sheared from an anisotropic stress state, which was close to the in situ condition. The intrinsic isotropic compression line (ICL*) for the Emmerstad clay was estimated from the general intrinsic normal compression line proposed by Burland (1990). The ICL* for the reconstituted soil is expressed as

$$e^* = 0.821 - 0.066 \ln p' \qquad (37)$$

The additional voids ratio sustained by soil structure was estimated from an oedometer test and the known ICL*. Values of the model parameters used in these simulations are listed in Table 5. Poisson's ratio of the soil skeleton ν^* is assumed as 0.25, as is commonly used in geotechnical practice for a clay skeleton. Parameters ω and γ were determined by curve fitting.

The initial state of the clay was ($\sigma'_1 = 41.5$ kPa, $\sigma'_2 = \sigma'_3 = 23.5$ kPa, $e = 1.155$). The initial structural yield surface was assumed to be an ellipse with the aspect ratio being M*. The initial vertical yield stress measured from the oedometer data is 110 kPa, which gives $p'_{y,i} = 98$ kPa, based on an empirical equation suggested by Liu and Carter (2002). To give an overall picture of the undrained behaviour of this clay, an additional simulation of the conventional triaxial extension test with OCR = $(p'_{co}/p'_i) = 1.6$ is also made.

Table 5 Model parameters for Emmerstad clay

M*	λ*	κ*	E^*_{IC}	ν*
1.37	0.066	0.006	0.821	0.25
b	C	ω	γ	
0.4	0.35	1.8	0.1	
Initial structural yield surface: ellipse with $p'_{y,i} = 98$ kPa and aspect ratio = M*.				

(a) Effective stress paths

(b) Stress and strain relationship
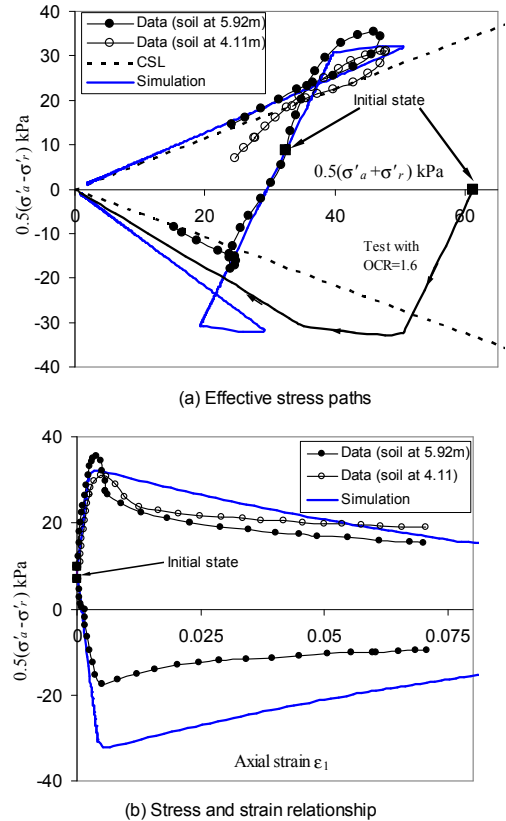
Figure 13 The behaviour of Emmerstad clay (Test data after Lacasse et al. 1985)

A comparison of the simulations and the experimental data for undrained triaxial shearing is shown in Figure 13. Overall, the proposed model gives a reasonably good description of the behaviour of the natural soft Emmerstad clay, which was sheared from an anisotropic stress state to failure.

The following observations are made regarding the soil behaviour and the model simulations.

(1) The strengths of the soil in triaxial extension stress states have been significantly over-predicted. This arises, at least in part, from the adoption of the Von Mises failure criterion, rather than the Mohr-Coulomb criterion.

(2) Laccase et al. (1985) observed that Emmerstad clay is extremely sensitive, with the sensitivity index varying from 60 upwards. This is confirmed by the simulations which predict the final strength of the soil as being almost negligible.

(3) Unlike most very soft clays, Emmerstad clay exhibits a significant amount of negative excess pore pressure when it softens, which is usually a feature of stiff clay behaviour (e.g., Vaughan 1994). This particular feature has been captured well by the SCC model through assigning a low value of γ and a high value of c relative to the initial value of the additional voids ratio Δe_i. As a result, the modified SCC model predicts greater sensitivity to the destructuring caused by increasing shear stress at states near the critical state than by increasing mean stress. Consequently, at the beginning of softening, the plastic volumetric deformation is controlled by the softening mechanism and is thus expansive, which leads to the development of negative pore pressure. The major portion of the additional voids ratio sustained by soil structure is reduced only near the end of the softening process when the current stress ratio approaches M* and a large amount of positive pore pressure is produced during this part of the process, as can be inferred from the simulations.

4 Dogs Bay carbonate sand

Experimental data observed for this sand were reported by Golightly and Hyde (1988). The maximum and minimum voids ratios for the carbonate sand are 1.83 and 0.98, respectively. Results have been reported for ten conventional triaxial undrained tests, each at a constant confining pressure. The initial voids ratio for all the tests was 1.0. All the samples were prepared by a similar method, involving the sand being dry-pluviated from a fixed height.

The model parameters identified for Dogs Bay carbonate sand are listed in Table 6. The size of the initial structural yield surface is 400 kPa and its shape is elliptical with the aspect ratio being M*. Values of parameters M*, λ*, e*$_{IC}$ and $p'_{y,i}$ were determined from the experimental data reported by Golightly and Hyde (1988). The value of Poisson's ratio ν* was assumed according to common practice in geotechnical engineering. The values for parameters E*, b, ω and γ were determined by curve fitting. The value of the initial additional voids ratio Δe_i can be calculated from equation (5) as the initial states of the soil specimens are known. The values of Δe_i for all the tests are negative.

Table 6 Model parameters for Dogs Bay carbonate sand

M*	λ*	E* (kPa)	e*$_{IC}$	ν*
1.75	0.135	100,000	1.87	0.25
b	c	ω	γ	
0.25	0	0.1	0.2	
Initial structural yield surface: ellipse with $p'_{y,i}$ = 400 kPa and aspect ratio = M*.				

Comparison between the theoretical simulations and the experimental data for four of the ten tests is shown in Figure 14. It is seen that overall the behaviour of the carbonate sand under monotonic shearing has been simulated reasonably well by the proposed SCC model and the main features of the complicated behaviour of

this sand are satisfactorily captured. The following observations are made.

(1) Although the relative density for the Dogs Bay carbonate sand tested was as high as 97%, the soil with the initial mean effective stress greater than 400 kPa behaves like a virgin yielding material.

(2) The soil shows a special feature in p' - q space (Figure 9a). For normally consolidated and lightly over-consolidated sand, the effective stress paths reach a strength of the critical state shear stress ratio through virgin yielding, and for heavily over-consolidated sand, the effective stress paths reach a strength given by the critical state shear stress ratio through softening. After that, the effective stress paths for all the samples travel upwards along the critical state line until the sand finally reaches the critical state of failure. During the last stage, large strength increase is achieved. This type of behaviour has also been observed for some other sands (e.g., Ishihara 1993).

(a) Effective stress paths

(b) Stress and strain relationship
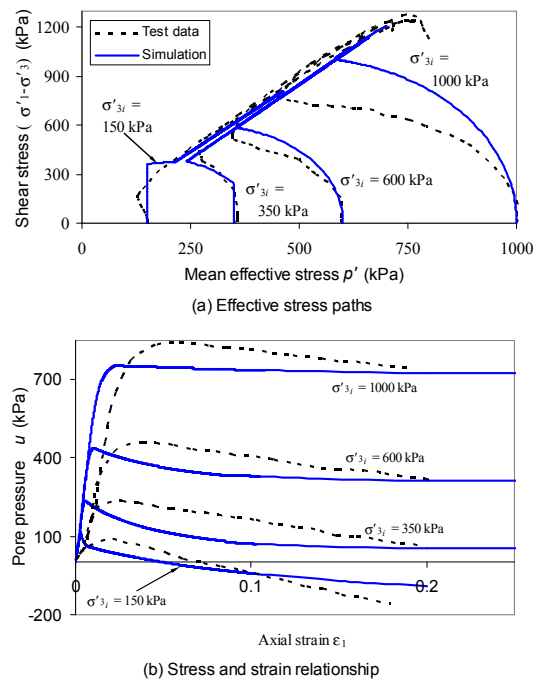
Figure 14 Undrained behaviour of Dogs Bay carbonate sand (test data after Golightly and Hyde 1988)

It can be seen that the SCC model has successfully captured the significant trends in the complicated behaviour of the carbonate sand. However, considerable quantitative discrepancies are observed between the simulations and the experimental data. Similar to that of the Modified Cam Clay model (Muir Wood 1990), the quantitative performance of the Structured Cam Clay model needs further improvement for describing in detail the behaviour of natural sands with various types and degrees of structure. It may also seen that the assumption of purely elastic deformation inside the virgin yield boundary is approximate for some materials, and hence

for those materials is only applicable for situations where soil deformation within the boundary is not the main concern.

5.5 Cemented Ariake clay

The undrained behaviour of cemented Ariake clay observed in tests performed by Horpibulsuk et al. (2004b) is simulated by the SCC model extended to include cementation effects. The tests were conventional triaxial tests at different confining pressures. The cement content for all tests was A_w = 9% by weight. Values of the model parameters identified are listed in Table 7.

Table 7 Model parameters for cemented Ariake clay

M*	λ*	E* (kPa)	e*$_{IC}$	ν*
1.85	0.44	20,000	4.37	0.25
b	C	ω	γ	C (kPa)
0.6	1.8	1.2	1	80
Initial structural yield surface: ellipse with $p'_{y,i}$ = 210 kPa and aspect ratio = M*.				

(a) Effective stress paths

(b) Stress and strain relationship
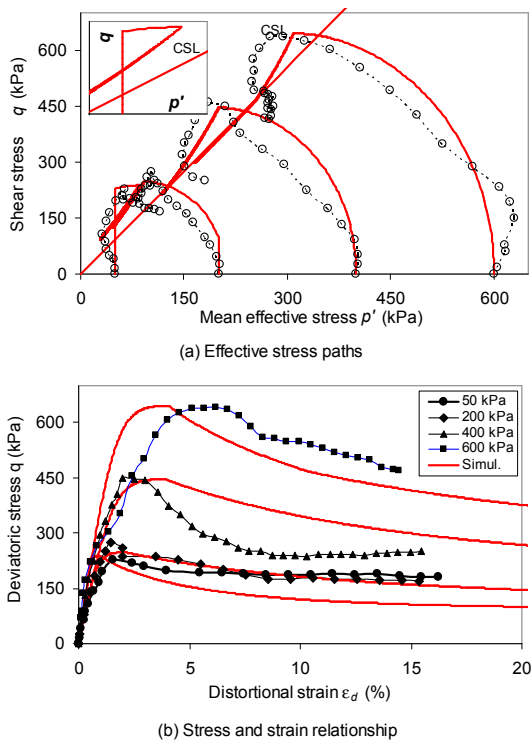
Figure 15 Stress and strain relationship for cemented Ariake clay for A_w = 9% (Test data from Horpibulsuk 2004b)

Four tests were simulated with the initial confining pressure being 50, 200, 400 and 600 kPa. A comparison of the undrained effective stress paths from the experimental data and model simulations is shown in Figure 15(a). A comparison of the stress and strain relationships of the clay is shown in Figure 15(b). Overall, the behaviour of cemented clay has been simulated highly satisfactorily considering that all model parameters were essentially identified according to their definitions, i.e., the triaxial test data were not back-fitted. The development of the pore pressure in this cemented clay is analyzed in detail here.

For cemented clay in a normal or lightly over-consolidated state, i.e., when the soil exhibits virgin yielding at low stress ratio, the undrained effective stress path in p' - q space first rises before bending towards the CSL, which indicates the development of positive pore pressure. Then it reaches a peak strength state. However, this peak strength state is not sustainable and instability occurs. The strength of the soil drops accompanied by the development of positive pore pressures and the breakdown of cementation. Finally, the soil reaches the ultimate failure state and thus becomes stable. During this process, the stress ratio is basically constant and the failure of the soil contributes to the production of positive pore pressure.

For cemented clay with a high over-consolidation ratio, the undrained effective stress path initially rises approximately vertically, which indicates elastic behaviour, and reaches a peak value; then softening occurs with the stress path moving to the right and towards the critical state line and with decreasing stress ratio. This indicates the generation of negative excess pore pressures. However, before reaching the final failure state the stress path changes its direction and travels downwards and approaches the critical state line from above, which indicates the generation of positive excess pore pressures (see the insert in Figure 15(a) for the test with σ'_3 = 100 kPa). This pattern of soil behaviour is usually not observed in reconstituted clays and hence most models of the Cam Clay family, developed for reconstituted soils, are generally incapable of describing such behaviour.

The structure of the soil created by induced cementation is very strong and the soil can sustain much higher voids ratio than the uncemented soil. For the Ariake clay in the tests, the initial voids ratio is over 4. For Ariake clay in a reconstituted state with much lower voids ratio, the corresponding critical state strength measured is close to zero. However, the final strength of the cemented clay is significant and also increases with cement content. This indicates that part of the structure associated with artificial cementation is meta-stable and thus cannot be removed by conventional loading. This very important and positive effect of cementation is well represented in the proposed model.

6. MODEL PREDICTIONS IN BOUNDARY VALUE PROBLEMS

The Structured Cam Clay model has been incorporated into the finite element program AFENA (Carter and Balaam 1995) and used to solve a variety of boundary value problems. In this section the application of the model to the prediction of the bearing behaviour of circular footings is considered. Parametric studies have been performed by Liyanapathirana et al. (2003a; 2003b; 2008) to identify which of the model parameters are most significant in determining the response of a footing on

structured soil, and therefore which of the parameters requires the most accurate determination. The results of the parametric study have also been summarized in the form of design guidelines, expressed as closed form expressions for predicting footing response.

6.1 Undrained bearing resistance

One of the important features of the mechanical behaviour of structured soils is the occurrence of a destructuring phase as these soils are loaded. During this phase, the structure of the soil may be completely or partially lost and only a small change in stress state may cause very large strains. Consequently, significant errors in prediction of foundation behaviour can arise if the influence of soil structure is not incorporated into these predictions.

Well-established formulae for determining the undrained bearing capacity of shallow circular foundations have been proposed by Terzaghi and Peck (1967), Davis and Booker (1973), Salençon and Matar (1982), Kusakabe et al. (1986) and Tani and Craig (1995). These take into account the foundation shape, size, depth of embedment and variation of soil properties with depth, but they do not directly take into account the influence of soil structure on the bearing resistance.

Geotechnical engineers have long experience in the use of a factor of safety in design, and generally they have been successful in designing shallow foundations on natural and man-made soils using this approach. The methods used generally ignore the effects of soil structure on its bearing behaviour. However, for special cases, such as offshore structures, where there is often less experience, incorporating the complex behaviour of structured soils directly in bearing capacity predictions may be very important. Therefore, the main objective of this section is to examine the significance of soil structure on the undrained bearing capacity of shallow foundations resting on the surface of structured soil deposits.

In particular, a series of numerical simulations have been carried out to investigate the influence of soil structure on the undrained (or immediate) load-displacement response of shallow foundations. Based on these numerical simulations, guidelines are provided to identify when the structural features of the soil become important in assessing the undrained (short-term) bearing capacity of shallow circular foundations. The factor, N_c, used in the classical bearing capacity theory, has been modified by incorporating directly the structural features of the soil to quantify the undrained bearing capacity.

6.2 Finite element model

The finite element mesh used for the analysis consisted of fifteen-noded cubic strain triangles, and a 16-point Gaussian quadrature was performed. According to Sloan and Randolph (1982), this element is capable of accurate computations in the fully plastic range during undrained loading in problems which involve axial symmetry. In all analyses presented in this paper, it is assumed that the contact between the footing and the soil is perfectly rough.

6.3 Effect of soil structure on bearing capacity

To study the effect of soil structure on the bearing capacity, a parametric study was carried out by varying the footing diameter and the model parameters which govern the structural features of the soil for typical examples of both stiff and soft clays. The values of other parameters were kept constant and they are the same as those given in Table 8.

Table 8 Properties of stiff and soft clay

Property	Stiff clay	Soft clay
λ^*	0.161	0.22
κ^*	0.033	0.022
M*	1.0	1.3
ν^*	0.2	0.4
e^*_{cs}	2.75	2.86
B	4.0	4.0
γ	0.5	0.5
ω	1.0	1.0
γ' (kN/m^3)	8.19	7.19

For reconstituted soils loaded under both drained and undrained conditions, it was found that for a unique value of the combined parameter $\gamma'B/p'^*_{co}$, the non-dimensional bearing pressure q_{av}/p'^*_{co} plotted against the non-dimensional footing settlement δ/B was almost the same, irrespective of the individual values of each variable. Here, q_{av} is the average applied footing pressure, δ is the footing settlement, B is the footing diameter and γ' is the effective unit weight of the soil.
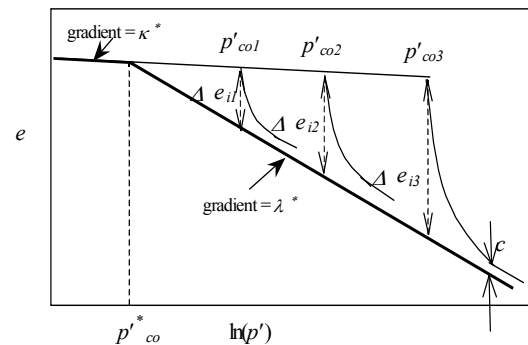
Figure 16 Variation of p'_{co} with Δe_i for structured soils

For a particular soil, the size of the yield surface of the structured soil, p'_{co}, is always greater than the size of the yield surface of the reconstituted soil, p'^*_{co}, due to the additional voids ratio sustained by the soil structure, Δe_i. The variation of p'_{co} depends on κ^*, λ^* and Δe_i, as illustrated in Figure 16, and is given by

$$p'_{co} = p'^*_{co} \exp\left(\frac{\Delta e_i}{\lambda^* - \kappa^*}\right) \qquad (38)$$

Therefore, for a particular soil the degree of structure with respect to the reconstituted soil can be defined by using either p'_{co}/p'^*_{co} or $\Delta e_i/(\lambda^* - \kappa^*)$. It was found that the influence of γ, ω and the destructuring index, b, do not have a significant influence on the undrained bearing capacity. Thus, in the parametric study the influence of soil structure has been studied by varying only $\Delta e_i/(\lambda^* - \kappa^*)$.

6.4 Bearing capacity of stiff structured clay

Figure 17 illustrates the influence of the degree of soil structure on the undrained bearing response of a 2 m diameter circular footing. Clearly, the bearing capacity reaches an ultimate value during undrained loading, in contrast to the approximate bilinear load-displacement response observed during drained loading of similar materials, as demonstrated later in this paper and by Liyanapathirana et al. (2003a, 2003b). This indicates that for these undrained cases the soil beneath the footing should fail in the general shear failure mode.
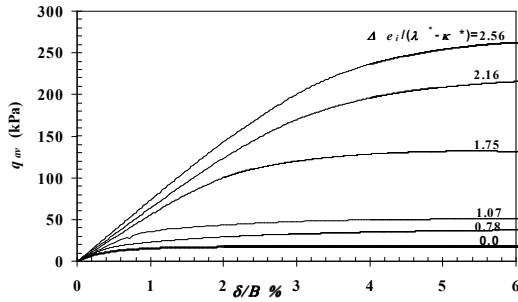
Figure 17 Variation of q'_{av} with $\Delta e_i/(\lambda^* - \kappa^*)$ for a 2m diameter circular footing on stiff clay

With an increase in the degree of soil structure, the bearing capacity increases significantly, e.g., when $\Delta e_i/(\lambda^* - \kappa^*)$ increases from 1.07 to 2.16, there is a four-fold increase in the bearing capacity of the footing. If the undrained bearing capacity is calculated based on the reconstituted soil properties, neglecting the structural properties of the soil, the predicted bearing capacity can be a very low value compared with the true theoretical load carrying capacity of the footing.

Figure 18 shows the non-dimensional bearing capacity, q_{av}/p'^*_{co}, obtained from the finite element analysis for different values of degree of soil structure, $\Delta e_i/(\lambda^* - \kappa^*)$, and $\gamma' B/p'^*_{co}$ for stiff clay. For the range of $\gamma' B/p'^*_{co}$ considered in the parametric study, it can be seen that the degree of soil structure has a significant influence on the bearing capacity of the foundation. Based on the above observation, an equation for the bearing capacity calculation can be formulated based on

the critical state and structural parameters of the soil, as follows

$$\frac{q_{av}}{p'^*_{co}} = \exp\left(1.3\frac{\Delta e_i}{\lambda^* - \kappa^*}\right)\left(\frac{\gamma' B}{p'^*_{co}}\right)^n \qquad (39)$$

where $n = 0.23\left(\dfrac{\Delta e_i}{\lambda^* - \kappa^*}\right)^{-0.25}$.

The new equation takes into account the influence of soil structure on the bearing capacity.
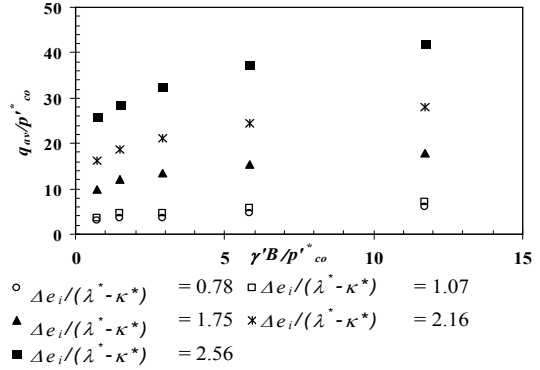
Figure 18 Variation of q'_{av}/p'_{co} with $\Delta e_i/(\lambda^* - \kappa^*)$ for a 2m diameter circular footing on stiff clay

6.5 Influence of degree of soil structure on undrained shear strength

The undrained shear strength of the soil, S_u, is an important parameter in determining the short term or undrained bearing capacity. However, the undrained shear strength is not a direct input parameter of the Structured Cam Clay model. For the Modified Cam Clay model, which simulates the constitutive behaviour of reconstituted soil, the undrained strength can be derived from the following equation (e.g., Zdravković and Potts 2003)

$$S_u = g(\theta)\cos(\theta)\frac{OCR}{6}\left(1+2K_o^{NC}\right)\left(1+B^2\right)\times$$
$$\left[\frac{2\left(1+2K_o^{OC}\right)}{\left(1+2K_o^{NC}\right)OCR\left(1+B^2\right)}\right]^{\kappa^*/\lambda^*} \qquad (40)$$

where $K_o^{NC} = 1 - \sin\phi'$, $\quad K_o^{OC} = K_o^{NC} OCR^{\sin\phi'}$ and $B = \dfrac{\sqrt{3}\left(1-K_o^{NC}\right)}{g\left(-30^o\right)\left(1+2K_o^{NC}\right)}$.

θ is the Lode angle, OCR is the overconsolidation ratio, and K_o^{NC} and K_o^{OC} are the coefficients of earth pressure at rest for a normally consolidated and an overconsolidated soil, respectively. If we assume a circular yield surface in the deviatoric plane, $g(\theta)$ can be replaced by $M^*/\sqrt{3}$.

For a structured soil $\Delta e_i/(\lambda^* - \kappa^*)$ increases with the degree of soil structure and p'_{co} is related to Δe_i according to Equation (38). The OCR of the soil is also related to soil structure and according to Equation (40), S_u increases

with OCR. Therefore, the influence of the degree of soil structure can be incorporated into the undrained shear strength of the soil via equation (40).

6.6 Bearing capacity of stiff clay

Figure 19 shows the variation of S_u with depth in the structured soil deposit for different values of $\Delta e_i / (\lambda^* - \kappa^*)$ and the corresponding OCR. In each case it is assumed that OCR is independent of depth. The ultimate bearing capacity of a surface foundation, q_u, is normally expressed in the form

$$q_u = N_c s_c S_{u_o} \tag{41}$$

where s_c is the shape factor, S_{uo} is the undrained shear strength of the soil at the ground surface, and N_c is the bearing capacity factor.
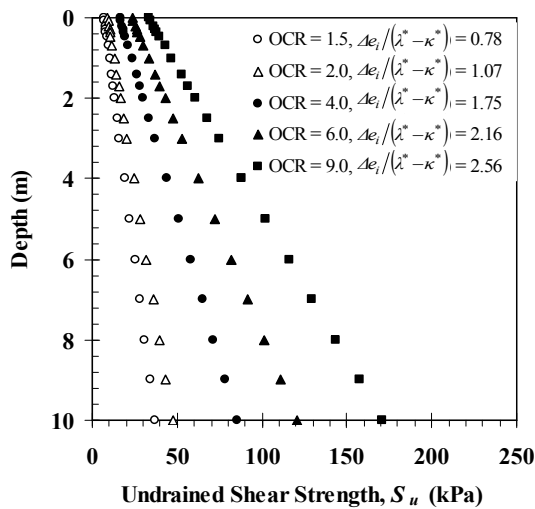
Figure 19 Undrained shear strength profiles for stiff clays

Based on plasticity theory, several authors have recommended values for N_c and s_c (or their product) as functions of kB/S_{uo}, where k is the gradient of S_u over the depth of the soil deposit, e.g., Salençon and Martar (1982), Kusakabe et al. (1986), Tani and Craig (1995) and Davis and Booker (1973). In Figure 20, reproduced from Liyanapathirana et al. (2003b), the bearing capacity obtained from selected plasticity solutions and the finite element analysis of the structured soil are compared. According to Terzaghi and Peck (1967), the value of N_c is 5.14 for a soil of uniform strength. Three other recommended values are also plotted in Figure 20. In these solutions, q_u/S_{uo} increases with kB/S_{uo}. However, according to Figure 20, in addition to kB/S_{uo}, q_u/S_{uo} depends on the individual values of S_{uo} or in other words on the OCR of the soil. Liyanapathirana et al. (2003a, 2003b) suggested that to sufficient accuracy this effect can be incorporated into the bearing capacity calculation as follows

$$\frac{q_u}{S_{uo}} = N_c s_c = \left[3.25 \ln\left(\frac{S_{uo}}{p_a}\right) + 13.2 \right]\left(\frac{kB}{S_{uo}}\right)^n \tag{42}$$

where $n = 0.14\left(\dfrac{S_{uo}}{p_a}\right)^{-0.2}$ and p_a is atmospheric pressure (≈ 100 kPa). If a value of S_{uo} is available for the intact undisturbed soil, i.e., the peak strength of the structured soil, then equation (39) can be used to obtain the ultimate bearing capacity. This may be more convenient than using the alternative, equation (40), which requires direct knowledge of the structural parameters of the soil.
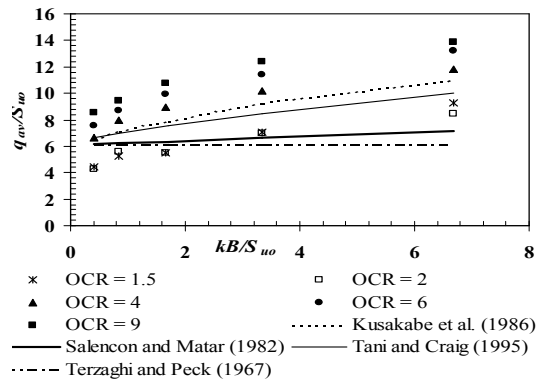
Figure 20 Comparison of bearing capacity obtained from SCC model with solutions based on plasticity theory

6.7 Bearing capacity of soft clay

Usually soft clay deposits have a crust above the ground water table and are close to normally consolidated below the water table. In this section the influence of a surface crust is studied for a shallow 2 m diameter circular foundation, and it is assumed that the water table is 2 m below the ground surface. The undrained shear strength profiles for the four cases considered by Liyanapathirana et al. (2003a and b) are shown in Figure 21. In the case of OCR = 1, there is no surface crust. In the other three cases, the OCR values at the ground surface are 3, 6 and 9, respectively, and each has a polynomial variation of strength above the water table. Below the water table however, it is assumed OCR = 1 for all four cases. Usually in soft clays, this surface crust provides the necessary strength to carry surface loading (e.g., Zdravković and Potts 2003). In each case, Δe_i was allowed to vary through the crust and values were calculated using equation (39), assuming $p'^*_{co} = 10$ kPa. Below the surface crust Δe_i was assumed to have constant value of 0.1.

Figure 22 shows the average bearing pressure with footing displacement predicted by Liyanapathirana et al. (2003a and b) for the cases given in Figure 21. The presence of the crust significantly increases the bearing capacity of the footing. When the OCR at the surface of the crust is 6, the bearing capacity has nearly doubled compared to the capacity without a crust. Unlike the stiff clay, for these soft clays, the bearing capacity does not

reach an ultimate value but continues to increase slowly with increasing footing displacement.
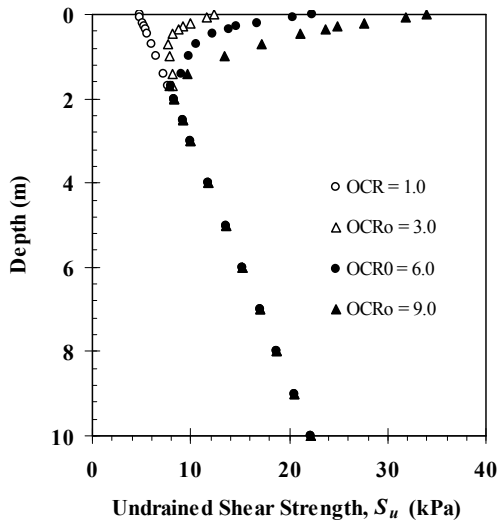
Figure 21 Undrained shear strength profiles for soft clays
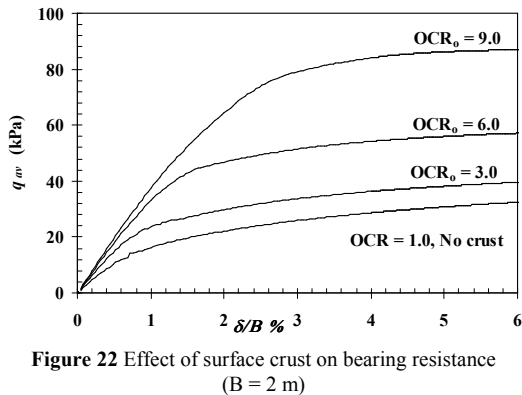
Figure 22 Effect of surface crust on bearing resistance (B = 2 m)

For soft clay deposits, it is not possible to compute q_u using the methods proposed by Salençon and Matar (1982), Kusakabe et al. (1986) and Tani and Craig (1995), because in all these methods the bearing capacity is a function of kB/S_{uo}. For these soft clays, the distribution of S_u is not a simple linear increase with depth, as assumed in the derivation of those methods. Therefore, the finite element results have been compared only with the predictions of the Terzaghi and Peck (1967) method.

Figure 23 shows the bearing capacity obtained from the finite element analysis by Liyanapathirana et al. (2003a and b) when the footing displacement is 10% of the footing diameter, and from the Terzaghi and Peck (1967) method. In the Terzaghi and Peck method (equation 24), the bearing capacity has been calculated using the undrained shear strength at the ground surface and the average undrained shear strength over the depth interval equivalent to the diameter of the footing. It is

clear that where there is a crust with OCR greater than about 3, the bearing capacity equation proposed by Terzaghi and Peck (1967) significantly over predicts the load carrying capacity of the foundation. However, if the OCR at the surface is less than or equal to about 3, the bearing capacity calculated using the Terzaghi and Peck equation matches reasonably well with the finite element results.
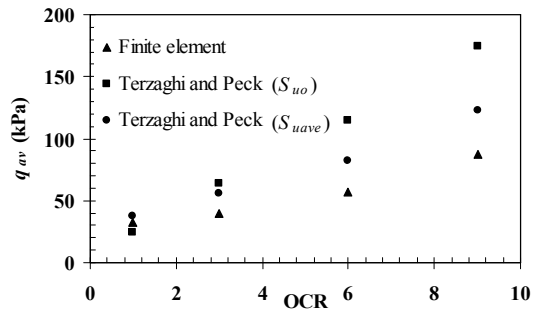
Figure 23 Bearing capacity for different OCR at surface of soft clay deposit
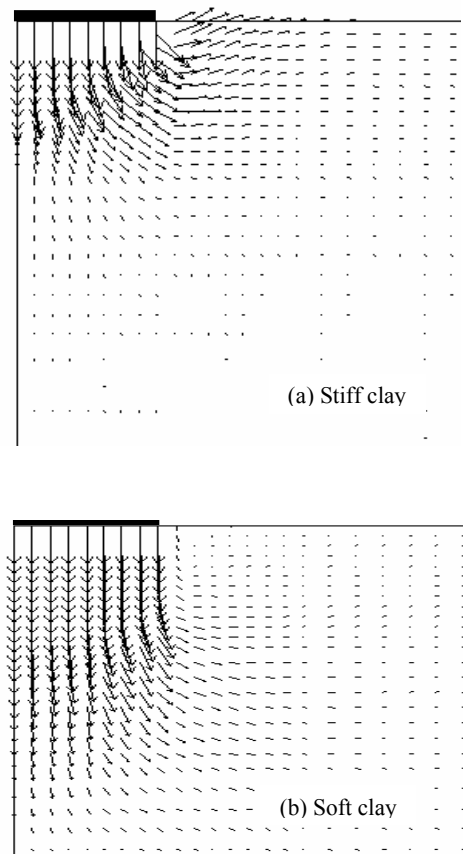
Figure 24 Incremental displacements

6.8 Failure mechanisms

Figures 24a and b show, respectively, the incremental soil displacements for stiff and soft clay deposits when the cumulative displacement of the footing is 7.5% of the footing diameter as predicted by Liyanapathirana et al. (2003s and b). The footing considered has a diameter of 2 m. The stiff clay deposit considered has an OCR of 6 throughout the soil deposit and the soft clay deposit considered has an OCR of 6 at the ground surface.

It can be seen that in stiff and soft clays, the failure mechanisms are not the same. In stiff clay, soil beneath the centre of the footing moves predominantly in the vertical direction, but towards the outer edge of the footing soil movement is predominantly in the radial direction and the soil heaves around the footing, similar to a general shear failure.

In soft clay, the soil flow pattern shown in Figure 24 (b) is different to that observed for stiff clay. Soil flow beneath the footing is predominantly in the vertical direction confined largely to a zone beneath the footing. Although some vectors are at an angle to the vertical, they do not show a flow pattern in a radial shearing zone. According to the load displacement response shown in Figure 22, no visible collapse is observed and a continuous increase in the vertical load is needed to maintain the footing movement in the downward direction. Therefore, it can be concluded that the deformation of the structured soft clay beneath the footing occurs predominantly as local shear failure under undrained conditions.

6.9 Long-term bearing resistance of structured soils

Accurate assessment of the bearing resistance of the ground is an important step in the process of evaluation of the stability and economy of structures. The bearing capacity of a footing is often mobilised as a shear failure that occurs within the soil supporting the footing. It is generally recognized that there are three principal modes of shear failure: general shear failure, local shear failure and punching shear failure.

Numerical analyses have also been carried out by Liyanapathirana et al. (2003a and b) to investigate the possible modes of failure for structured soils deforming under fully drained conditions. Figure 25 shows a normalized plot of the mobilized bearing pressure against the footing settlement for a 5 m diameter rigid circular footing resting on a typical structured soil deposit. No visible collapse is observed and a continuous increase in vertical load is needed to maintain the footing movement in the downward direction. Figure 26 shows the cumulative displacement vectors at a displacement of 10% relative to the diameter of the footing. The displacement vectors are predominantly in the vertically downward direction. Although a few vectors are at an angle to the vertical, they do not show a flow pattern in a radial shearing zone. Therefore, it can be concluded that the deformation of the structured soil beneath the footing occurs predominantly as a punching shear failure under fully drained conditions.
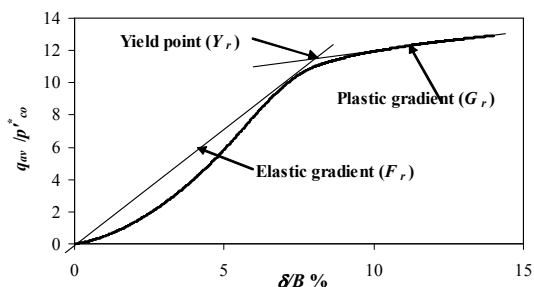
Figure 25 Mobilization of bearing resistance with footing movement
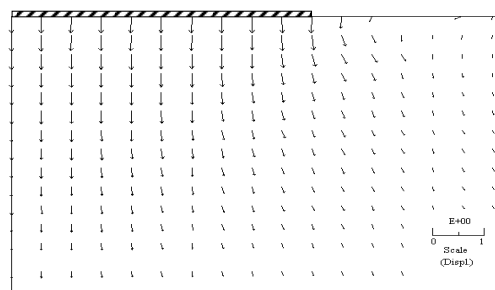
Figure 26 Cumulative displacement vectors beneath the footing at a displacement of $0.1B$

6.10 Prediction of drained bearing response curve

Since failure of the soil beneath the footing occurs as a punching shear, the mobilised bearing pressure continuously increases with the footing movement, apparently without reaching an ultimate bearing capacity, at least within the bounds of a small displacement approach. For punching shear, the bearing pressure mobilized at a displacement of 10% of the footing diameter is often defined as the "bearing capacity". However, this is an arbitrary value. Sharp and Seters (1988) and Islam (1999) showed that for punching shear, bearing pressure curves can be approximated by bilinear relationships. Although both sections of the curve involve elasto-plastic behaviour, the first section of the curve represents predominantly elastic penetration of the footing and the second represents predominantly plastic penetration of the footing. Therefore the first section of the curve is termed as 'elastic' and the second section is termed as 'plastic'. If gradients of the elastic (F_r) and plastic (G_r) parts and the yield point (Y_r), as shown in Figure 25, are known, an approximate curve of dimensionless bearing pressure $q_{av}/p_{co}'^*$ versus dimensionless displacement (δ/B) can be predicted, where q_{av} is the average applied footing pressure, $p_{co}'^*$ is the intercept of the current structural yield surface on the mean effective stress axis, δ is the footing settlement and B is the footing diameter. Hence, the bearing pressure can be obtained for any vertical movement of the footing, instead of assigning an arbitrary value as the ultimate bearing capacity.

In the following sections, a method is outlined to obtain the long-term (fully drained) bearing response of circular footings resting on structured soil deposits. First the bearing response is predicted for the same soil in the reconstituted state, neglecting the structural properties of the soil. After that, this curve is modified to obtain the bearing response for the structured soil, incorporating the structural properties of the soil.

6.10.1 Bearing response of reconstituted soil

In an earlier study, Liyanapathirana et al. (2008) demonstrated that the drained bearing response curve for reconstituted soils could be approximated by closed-form expressions. Only three equations are needed to represent the combined influence of the critical state parameters on F_r, Y_r and G_r, which define the complete bearing response of the reconstituted soil. Subsequently, the influence of structural properties of the soil will be incorporated into these three equations to obtain expressions for F_s, Y_s and G_s, which describe the response of a structured soil.

A simple multiplicative technique has been used to derive equations for F_r, Y_r and G_r incorporating the influence of all reconstituted soil properties and the dimensionless parameter $\gamma'B/p_{co}'^*$. For the elastic gradient, F_r, only κ^*, v^* and e_{cs}^* have a significant influence. Since the influence of κ^* on the bearing response was derived assuming $v^* = 0.25$ and $e_{cs}^* = 1.8$, an expression for F_r that incorporates other values of v^* and e_{cs}^* is derived assuming that the effect of each parameter is multiplicative, as follows

$$F_r = (F_r)_{\kappa^*} \frac{(F_r)_{v^*}}{(F_r)_{v^*=0.25}} \frac{(F_r)_{e_{cs}^*}}{(F_r)_{e_{cs}^*=1.8}} \qquad (43)$$

By substituting appropriate expressions for $(F_r)_{\kappa^*}$, $(F_r)_{v^*}$ and $(F_r)_{e_{cs}^*}$, Lyanapatirana et al. (2008) showed that the elastic gradient, F_r, can be represented in terms of $\gamma'B/p_{co}'^*$, κ^*, v^* and e_{cs}^* and as follows

$$F_r = (\kappa^*)^{-1}(0.97 - 1.6v^*)(e^*_{cs})^{0.7}\left(\frac{\gamma'B}{p^*{}'_{co}}\right)^{0.6} \qquad (44)$$

In the derivation of Equation (44), it has been demonstrated that the influence of λ^* and M^* on the elastic gradient, F_r, is small enough to be ignored. The accuracy of this approach will be demonstrated later in the paper.

The yield point, Y_r, varies only with M^* and $\gamma'B/p_{co}'^*$ and is given by

$$Y_r = (Y_r)_{M^*} = (M^*)^{1.25}\left(\frac{\gamma'B}{p^*{}'_{co}}\right)^m \qquad (45)$$

where $m = 0.25(M^*)^{-0.75}$.

The plastic gradient, G_r, varies with three parameters λ^*, M^* and e_{cs}^*. Therefore, similar to F_r, an equation for G_r can be derived as shown below

$$G_r = (G_r)_{\lambda^*} \frac{(G_r)_{M^*}}{(G_r)_{M^*=1.2}} \frac{(G_r)_{e_{cs}^*}}{(G_r)_{e_{cs}^*=1.8}}$$

$$= 1.72(M^*)^3(\lambda^*)^{0.4}(e_{cs}^*)^{0.6}\left(\frac{\gamma'B}{p_{co}'^*}\right)^{\left(0.25(\lambda^*)^{-0.6} + 0.75(M^*)^{-0.6} + 0.72\right)}$$

$$(46)$$

Equations (44), (45) and (46) can be used to obtain values for F_r, Y_r and G_r for a circular footing of any diameter if the intrinsic soil properties κ^*, λ^*, M^*, v^* and e_{cs}^* are known.

6.10.2 Bearing response of structured soil

The influence of soil structure on the long-term (fully drained) bearing response is now studied by varying the parameters, which govern the structural features of the soil, i.e., b, Δe_i, ω and p_{co}' for different values of $\gamma'B/p_{co}'^*$.

As shown in Figure 16, for a given structured soil, the size of the yield surface, p_{co}', and the parameter $\Delta e_i/(\lambda^* - \kappa^*)$ are linked and their values can be related to the size of the yield surface for the same soil in a reconstituted state, $p_{co}'^*$, as shown previously in equation (38).

Hence, the parameter $\Delta e_i/(\lambda^* - \kappa^*)$ takes into account the combined influence of both Δe_i and p_{co}' for a particular soil and can be used to define the degree of soil structure with respect to the same soil in a reconstituted state. It is convenient to define an additional parameter, $\Delta e'_i$, as follows

$$\Delta e' = \Delta e_i / (\lambda^* - \kappa^*) \qquad (47)$$

Finite element analyses carried out show that the influence of ω on the long-term bearing capacity is not significant. Therefore, in this section the influence of soil structure on the bearing response of a particular footing is studied by varying only the destructuring index, b, and the degree of soil structure defined by $\Delta e'_i$.

6.10.3 Influence of degree of soil structure on bearing response

Figure 27 shows the influence of $\Delta e'_i$ on the bearing capacity for a 5 m diameter surface circular footing when b is 0.25. As $\Delta e'_i$ increases, the soil shows much stiffer response. For example, when $\Delta e' = \Delta e_i/(\lambda^* - \kappa^*)$ changes from 1.5 to 2.5, the bearing resistance at a footing displacement equivalent to 12% of the footing diameter shows a three fold increase. If soil structure is not taken into account, the predicted bearing resistance is only about half of that obtained for a structured soil for which $\Delta e'_i$ is 1.5. According to Figure 27, $\Delta e'_i$ has a significant influence only on the elastic gradient, F_s, and the yield point, Y_s, of the bearing response curve for structured soils. For different values of $\Delta e'_i$ the plastic portions of each curve are virtually parallel to each other, and so the influence of $\Delta e'_i$ on the plastic gradient can be ignored.
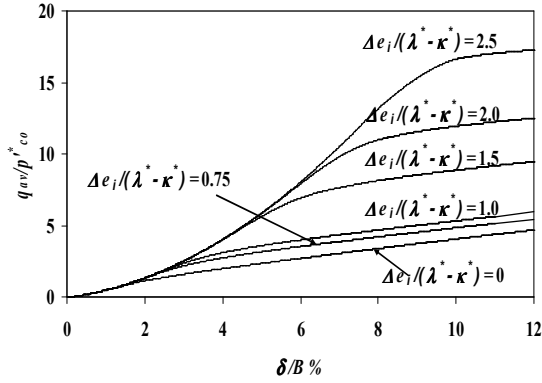
Figure 27 Influence of $\Delta e_i/(\lambda\text{*-}\kappa\text{*})$ on the bearing response (B = 5 m).
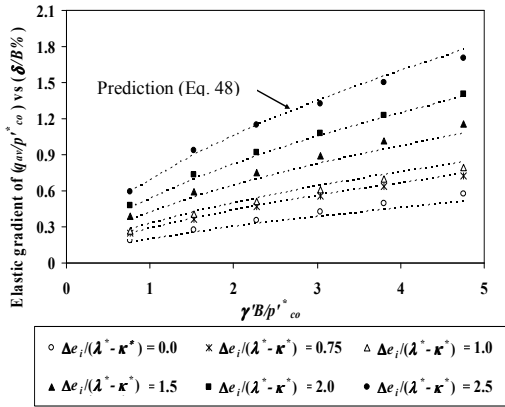
Figure 28 Variation of Elastic gradient, F_s, with $\Delta e_i/(\lambda\text{*-}\kappa\text{*})$ and $\gamma'B/p'\text{*}_{co}$.
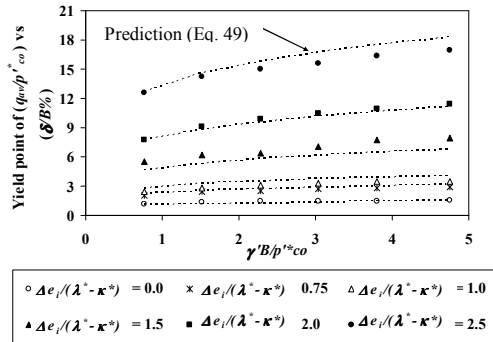
Figure 29 Variation of Yield point, Y_s, with $\Delta e_i/(\lambda\text{*-}\kappa\text{*})$ and $\gamma'B/p'\text{*}_{co}$.

Figures 28 and 29 show the combined influence of $\Delta e'_i$ and $\gamma'B/p_{co}^{'*}$ on the yield point, Y_s, and the elastic gradient, F_s. When $\Delta e'_i \leq 1$, the influence of soil structure on the bearing response can be ignored. For $\Delta e'_i > 1$, the influence of soil structure on bearing resistance is significant and should be incorporated in the

determination of the bearing response. Also, the influence of soil structure is more significant for larger values of $\gamma'B/p_{co}^{'*}$. Based on Figures 28 and 29, the variations of the elastic gradient and yield point with $\gamma'B/p_{co}^{'*}$ and $\Delta e'_i$ are given by

$$\left(F_s\right)_{\Delta e'_i} = 20\exp\left(0.5\Delta e'_i\right)\left(\frac{\gamma'B}{p'_{co}}\right)^{0.6} \tag{48}$$

$$\left(Y_s\right)_{\Delta e'_i} = 1.1\exp\left(\Delta e'_i\right)\left(\frac{\gamma'B}{p'_{co}}\right)^{0.2} \tag{49}$$

6.10.4 Influence of destructuring index on bearing response

The destructuring index, b, of a structured soil defines the rate at which soil structure is lost during yielding. For soils with higher values of destructuring index, the structure is completely lost with only a small change in the stress state beyond first yield. Figure 30 shows the influence of the destructuring index on bearing response for a 5 m diameter surface circular footing when the degree of soil structure, $\Delta e'_i$, is 1.5. It can be seen that b has an influence on the bearing capacity only beyond the yield point where the soil behaviour is predominantly plastic.
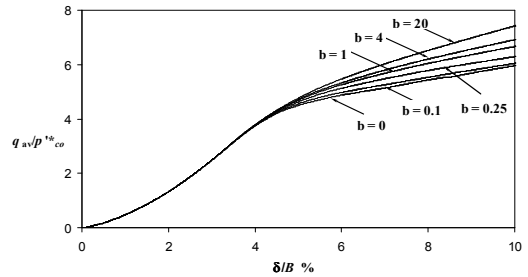
Figure 30 Influence of destructuring index, b, on the bearing response ($B = 5$ m).
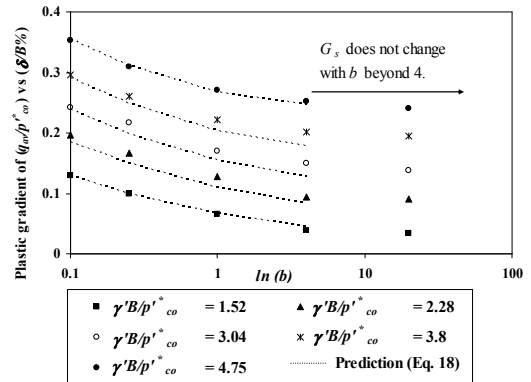
Figure 31 Variation of Plastic gradient, G_s, with $\Delta e_i/(\lambda\text{*-}\kappa\text{*})$ and $\gamma'B/p'\text{*}_{co}$.

Figure 31 shows the variation of plastic gradient with the logarithm of b for a range values of $\gamma'B/p_{co}'^*$. For all values of $\gamma'B/p_{co}'^*$, the plastic gradient reduces with increasing b and the change in plastic gradient with b is significant only when $b \le 4$. The finite element predictions given in Figure 31 can be fitted quite well to the following equation

$$(G_s)_b = 4(b)^{-0.36}\left(\frac{\gamma'B}{p_{co}'}\right)^{1.22(b)^{0.14}} \tag{50}$$

6.10.5 Bearing response curve for structured soil

Previously a method was suggested to obtain the bearing response curve for any reconstituted soil based on the intrinsic soil parameters, neglecting the influence of soil structure. In this section, expressions derived for a reconstituted soil are modified by incorporating the influence of soil structure.

According to the previous results, only the degree of soil structure has an influence on the elastic gradient and the yield point and this influence can be described to sufficient accuracy by

$$\frac{F_s}{F_r} = \frac{(F_s)_{\Delta e_i'}}{(F_s)_{\Delta e_i'=0}} = \exp(0.5\Delta e_i') \tag{51}$$

The plastic gradient of the bearing response curve is influenced significantly only by the destructuring index, b. According to Figure 27, when b is 0.25, the plastic gradients are nearly the same for all values of $\Delta e_i' = \Delta e_i/(\lambda^* - \kappa^*)$, in which case the influence of b on plastic gradient of the bearing response curve for a structured soil can be represented by

$$\frac{Y_s}{Y_r} = \frac{(Y_s)_{\Delta e_i}}{(Y_s)_{\Delta e_i'=0}} = \exp(\Delta e_i') \tag{52}$$

When applying this method, first F_r, Y_r and G_r have to be calculated using Equations (44), (45) and (46) respectively, based on the intrinsic properties of the reconstituted soil. If $\Delta e_i' \le 1$, the influence of degree of soil structure on bearing resistance can be ignored. If $\Delta e_i' > 1$, equations (51) and (52) can be used to compute F_s and Y_s. Finally, Equation (50) can be used to incorporate the influence of the destructuring index, b, on the plastic gradient of the bearing response curve, G_s.

6.11 Validation of the method for predicting drained bearing response

In order to validate the capability of the proposed method for predicting the long-term or drained bearing response of surface circular footings, plate load tests carried out by Consoli et al. (1998) have been considered. These tests were carried out in homogeneous lightly cemented residual soils in Southern Brazil. The upper surface soil at this site consisted of 4 m of lightly cemented homogeneous sandy silty red clay. Below that there was a 2 m thick layer of highly cemented red silty clay. The tests were carried out using rigid circular steel plates to load the soil at a depth of 1.2 m below the ground level. There were no embedment effects on the footing response because the upper 1.2 m of soil was removed over a large area of the test site.

Circular plate load tests carried out for 45 cm and 60 cm diameter plates have been simulated using the finite element method and the approximate method described previously. The values of soil parameters used to simulate these tests are given in Table 9. Figures 32 and 33 show, respectively, the results of plate load tests for 60 cm and 45 cm rigid steel plates.

Table 9 Model parameters for Dogs Bay carbonate sand

M*	λ*	κ*	e_{cs}^*	ν*
1.72	0.22	0.002	3.2	0.4
b	c	ω	γ	Δe_i
0.08	0	1	0	0.5
Initial structural yield surface: At ground surface $p_{co}' = 400$ kPa and $dp_{co}'/dz = 10$ kPa/m, bulk unit weight = 20 kN/m³				
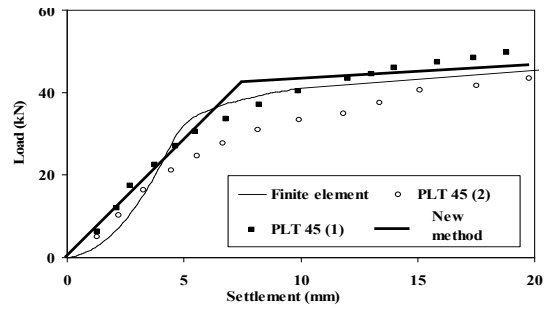
Figure 32 Predicted bearing response using the new method for 60 cm diameter footing
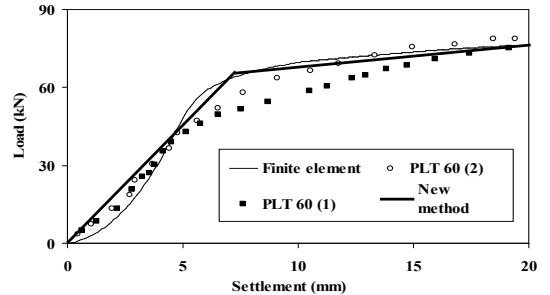
Figure 33 Predicted bearing response using the new method for 45 cm diameter footing

When using the new method, firstly the gradients and the yield pressure are calculated assuming reconstituted soil properties. Next, based on the degree of soil structure and the destructuring index, the gradients and the yield pressure for the structured soil can be obtained. Finally, these values can be used to obtain the bearing response of the circular footing on the structured soil. According to the parameter values given in Table 9, the degree of soil structure, $\Delta e_i' = \Delta e_i/(\lambda^* - \kappa^*)$, for the cemented soil is 2.3. Since $\Delta e_i' > 1$, the influence of degree of soil structure on the bearing response is significant and it should be incorporated into the values

calculated for F_s and Y_s. Also, the influence of the destructuring index, b, has to be incorporated into the value selected for G_s.

Equations (44), (45) and (46) can be used to obtain F_r, Y_r and G_r, respectively. For the cemented soil, when $B = 0.45$ m, it is found that $F_r = 2.6$, $Y_r = 160$ and $G_r = 20$, and when $B = 0.6$ m, $F_r = 310$, $Y_r = 1.7$ and $G_r = 20$. Next, based on the structural properties of the soil, F_s/F_r, Y_s/Y_r and G_s/G_r can be obtained from Equations (52), (51) and (50), respectively. These ratios are independent of footing size. Therefore, for $B = 0.45$ m and $B = 0.6$ m, $F_s/F_r = 3.1$, $Y_s/Y_r = 9.9$ and $G_s/G_r = 1.8$. Figures 32 and 33 show the bearing response obtained for the footings using the new approximate method. Only displacements up to 20 mm have been plotted in order to see more closely the level of agreement between elastic gradients obtained from the new method, finite element results and the field tests. The bilinear approximation predicted for the structured soil from the new method agrees well with the bearing pressure curve obtained from the finite element analysis and the experimental results of the plate load test.

7. CONCLUSIONS

An advanced constitutive model, the Structured Cam Clay, has been introduced in this paper. The SCC is a relatively simple predictive constitutive model suitable for the solution of boundary value problems encountered in geotechnical engineering practice. The model is formulated within the framework of critical state soil mechanics. It has successfully unified the mechanical properties of clays in reconstituted states, naturally structured states and artificially cemented states into one consistent theoretical framework, the Structured Cam Clay theoretical framework. The applicability of the model for predicting the mechanical behaviour of a range of structured soils in both single element tests and boundary value problems has been described. It has also been shown that SCC can be extended for complicated material behaviour such as that of artificially cemented clays.

The influence of soil structure on the bearing response of circular footings under both undrained and fully drained conditions has also been investigated using this model. It was found that for undrained conditions the ultimate bearing resistance depends on the properties defining soil structure at the stress-strain level. Under fully drained conditions, deformation of the soil beneath the footing occurs as punching shear. A parametric study has been carried out by varying those parameters which characterize the structural features of the soil. A novel method has been presented to obtain the relationship between the bearing pressure and footing displacement for a circular footing resting on a structured soil deposit. Application of the new method has been demonstrated using field plate load tests carried out on cemented residual soil in Southern Brazil. The bilinear bearing pressure curves predicted using the new method show very good agreement with the field plate load tests and finite element simulations. This suggests that the approximate method presented in this paper could be quite useful for predicting the bearing response of footings on structured soil.

REFERENCES

[1] Airey D.W. (1993), "Triaxial Testing of Naturally Cemented Carbonate Soil", *J. Geotechnical Engineering*, ASCE, Vol. 119(9), pp.1379-1398.

[2] Arces M., Nocilla N., Aversa S. and Cicero G.L. (1998). Geological and geotechnical features of the Calcarenite di Marsala. *The Geotechnics of Hard Soils - Soft Rocks*, Evangelista and Picarelli (eds): 15-25.

[3] Balasubramanian, A. S. & Hwang, Z. M. (1980). Yielding of weathered Bankok clay. *Soils and Foundations* 20, No. 2, 1–15.

[4] Burland, J.B. (1990). On the compressibility and shear strength of natural soils. *Géotechnique* 40 No. 3, 329–378.

[5] Carter, J.P. & Balaam, N.P. (1995). *AFENA User Manual, Version 6*, Centre for Geotechnical Research, University of Sydney.

[6] Carter J.P., Airey D.W. and Fahey M. (2000). A review of laboratory testing of calcareous soils. *Engineering for Calcareous Sediments*, Al-Shafei (*ed*). 2: 401-431.

[7] Carter, J.P. & Liu, M.D. (2005). Review of the structured cam clay model, *Geo-Frontiers*, Austin, Texas, Jan 24-25, ASCE.

[8] Clough, G.W., Sitar, N., Bachus, R.C. & Rad, N.S. 1981. Cemented sands under static loading. *Journal of Geotechnical Engineering Division, ASCE* 107(GT6): 799-817.

[9] Cotecchia F. & Chandler R.J. (1997). The influence of structure on the pre-failure behaviour of a natural clay, *Géotechnique* 47, No. 3, 523-544.

[10] Cuccovillo, T. & Coop, M.R. (1999). On the mechanics of structured sands. *Géotechnique* 49, No. 6, 741–760.

[11] Davis, E.H. & Booker, J.R. (1973). The effect of increasing strength with depth on the bearing capacity of clays. *Géotechnique* 23, No. 4, 551-562.

[12] Desai C.S. (2001). *Mechanics of Materials and Interfaces: The Disturbed State Concept*, CRC Press, Boca Raton.

[13] Diaz-Rodriguez J.A., Leroueil S. and Aleman J.D. (1992). Yielding of Mexico City clay and other natural clays. *J. Geotechnical Engineering*, ASCE. 118(7): 981-995.

[14] Graham J. and Li C.C. (1985). Comparison of natural and remoulded plastic clay. *J. Geotechnical Engineering*, ASCE: 111(7): 865-881.

[15] Gens, A. & Nova, R. (1993). Conceptual bases for a constitutive model for bonded soils and weak rocks. In: *Geotechnical engineering of hard soils – soft rocks*. Edited by A. Anagnostopoulos, F. Schlosser, N. Kalteziotis & R. Frank. A. A. Balkema, Rotterdam. Vol. 1, pp. 485–494.

[16] Golightly C.R. & Hyde A.F.L. (1988). Some fundamental properties of carbonate sands. In: *Engineering for Calcareous Sediments*, Jewell et al. editors, pp.69-78.

[17] Horpibulsuk S., (2001), *Analysis and Assessment of Engineering Behavior of Cement Stabilized Clays*, Ph.D. dissertation, Saga University, Saga, Japan.

[18] Horpibulsuk, S., Bergado, D.T., and Lorenzo, G.A. (2004a), "Compressibility of cement admixed clays at high water content", *Geotechnique*, Vol.54, No.2, pp.151-154.

[19] Horpibulsuk S., Miura N., and Bergado D.T., (2004b), "Undrained shear behaviour of cement admixed clay at high water content", *Journal of Geotechnical and Geoenvironmental Engineering*, ASCE, Vol. 130(10), pp.1096-1105.

[20] Horpibulsuk, S., Miura, N., and Nagaraj, T.S. (2005), "Clay-water/cement ratio identity of cement admixed soft clay", *Journal of Geotechnical and Geoenvironmental Engineering*, ASCE, Vol.131, No.2, pp.187-192.

[21] Huang J.T. and Airey D.W. (1998), "Properties of an artificially cemented carbonate sand", *Journal of Geotechnical and Geoenvironmental Engineering*, ASCE, Vol.124, No.6, pp.492-499.

[22] Ishihara, K. (1993). Liquefaction and flow failure during earthquakes. *Géotechnique* 43, No. 3, 351–415.

[23] Islam, K. (1999). *Constitutive models for carbonate sands and their application to footing problems*. PhD thesis, Centre for Geotechnical Research, University of Sydney, Australia.

[24] Ismail M.A., Joer H.A., Randolph M.F. and Sin W.H. (2002), "Effect of cement type on shear behaviour of cemented calcareous soil", *J. Geotechnical Engineering*, ASCE, Vol. 128(6), pp.520-529.

[25] Kasama, K., Ochiai, H. and Yasufuku, N. (2000), "On the stress-strain behaviour of lightly cemented clay based on an extended critical state concept". *Soils and Foundations*, Vol.40, No.5, pp.37-47.

[26] Kavvadas, M. & Amorosi, A. (2000). A constitutive model for structured soils. *Géotechnique* 50, No. 3, 263–273.

[27] King, R. & Lodge, M. (1988). North West shelf development – the foundation engineering challenge. In: *Proceedings of the International Conference on Calcareous Sediments*, Vol. 2, p. 333–342.

[28] Kusakabe, O., Suzuki, H. & Nakase, A. (1986). An upper bound calculation on bearing capacity of a circular footing on a non-homogeneous clay, *Soils and Foundations* 26, No. 3, 143-148.

[29] Lacasse S., Berre T. & Lefebvre G. (1985). Block sampling of sensitive clays. In: *Proceedings 11th International Conference Soil Mechanics and Foundation Engineering*, Vol. 2, pp.887-892.

[30] Lagioia, R. & Nova, R. (1995). An experimental and theoretical study of the behaviour of a calcarenite in triaxial compression. *Géotechnique* 45, No. 4, 633–648.

[31] Leroueil, S. & Vaughan, P.R. (1990). The general and congruent effects of structure in natural soils and weak rocks. *Géotechnique* 40, No. 3, 467–488.

[32] Liu, M.D. & Carter, J.P. (1999). Virgin compression of structured soils. *Géotechnique* 49, No. 1, 43–57.

[33] Liu, M.D. & Carter, J.P. (2000a). Modelling the destructuring of soils during virgin compression, *Géotechnique*, 50, No. 4, 479-483.

[34] Liu M.D. and Carter J.P. (2000b). On the volumetric deformation of reconstituted soils. *Int. J. for Numerical and Analytical Methods in Geomechanics*. 24(2): 101-133.

[35] Liu, M.D. & Carter, J.P. (2002). A Structured Cam Clay model. *Canadian Geotechnical Journal* 39, No. 6, 1313–1332.

[36] Liu, M.D. & Carter, J.P. (2003). The volumetric deformation of natural clays, *International Journal of Geomechanics*, ASCE, 3, No. 4, 236-252.

[37] Liyanapathirana, D.S., Liu, M.D., Airey, D.W. & Carter, J.P. (2003a). Predicting the behaviour of foundations on structured soils. *Proceedings XIIIth European Conference on Soil Mechanics and Geotechnical Engineering*, Prague, Czech Republic, Vol. 2, 255-260.

[38] Liyanapathirana, D.S., Carter, J.P. & Airey, D.W. (2003b). Bearing response of shallow foundations on structured soils. In: *Proceedings International Conference on Foundations: Innovations, Observations, Design and Practice*, Dundee, 521-530.

[39] Liyanapathirana, D.S., Carter, J.P. & Airey, D.W. (2008). Drained bearing response of shallow foundations on structured soils, *Computers and Geotechnics*, doi:10.1016/ j.compgeo.2008.04.004.

[40] Muir Wood, D. (1990). *Soil behaviour and critical state soil mechanics*. Cambridge University Press.

[41] Potts, D.M. & Zdravkovic, L. (1999). *Finite element analysis in geotechnical engineering: theory*. Thomas Telford, London.

[42] Potts, D.M., Jones, M.E. & Berget, O.P. (1988). Subsidence above the Ekofisk oil reservoirs. In: *Proceedings of the 5th international conference on the behaviour of offshore structures*, Trondheim, Vol. 1, p. 113–127.

[43] Roscoe, K.H. & Burland, J.B. (1968). On the generalised stress–strain behaviour of 'wet' clay. In: Heyman, J. & Leckie, F.A., editors. *Engineering plasticity*. Cambridge: Cambridge University Press; pp. 535–609.

[44] Rotta G.V., Consoli N.C., Prietto P.D.M., Coop M.R. & Graham J. (2003), "Isotropic yielding in an artificially cemented soil cured under stress", *Géotechnique*, Vol. 53, No.5, pp.493-501.

[45] Rouainia, M. & Muir Wood, D. (2000). A kinematic hardening model for natural clays with loss of structure. *Géotechnique* 50, No. 2, 153–164.

[46] Salençon, J. & Matar, M. (1982). Bearing capacity of axially symmetrical shallow foundations. *Journal Mechanique Theorique et Appliqueé*, 1(2), 237-267.

[47] Schofield, A.N. & Wroth, C.P. (1968). *Critical state soil mechanics*. McGraw-Hill, London.

[48] Sharp, D.E. & Seters, A.J. (1988). Results and evaluation of plate load test results. In: *Proceedings of the international conference on calcareous sediments*, Perth, Australia, p. 473–483.

[49] Sloan, S.W. & Randolph, M.F. (1982). Numerical prediction of collapse collapse loads using finite element methods, *International Journal of Numerical and Analytical methods in Geomechanics*, 6, 47-76.

[50] Tani, K. & Craig, W.H. (1995). Bearing capacity of circular foundations on soft clay of strength increasing with depth, *Soils and Foundations* 35. No. 4, 21-35.

[51] Terzaghi, K. (1943). *Theoretical soil mechanics*. John Wiley and Sons Inc. New York.

[52] Terzaghi, K. & Peck, R.B. (1967). *Soil Mechanics in Engineering Practice*, John Wiley and Sons, New York.

[53] Vaughan, P.R. (1994). Assumption, prediction and reality in geotechnical engineering, *Géotechnique* 44, No. 4, 573-609.

[54] Walker, L.K. & Raymond, G.P. (1969). Anisotropic consolidation of Leda clay. *Canadian Geotechnical Journal*, 6, 271–286.

[55] Wong R.C.K. (1980), "Swelling and softening behaviour of La Biche shale", *Canadian Geotechnical J.*, Vol. 35, pp.206-221.

[56] Whittle, A.J. (1993). Evaluation of a constitutive model for overconsolidated clays. *Géotechnique* 43, No. 2, 289–314.

[57] Wissa, A.E.Z., Ladd, C.C. & Lambe, T.W. 1965. Effective stress strength parameters of stabilized soils. *Proc. 6th International Conference on Soil Mechanics and Foundation Engineering*, 412-416.

[58] Yong, R.N. & Nagaraj, T.S. (1977). Investigation of fabric and compressibility of a sensitive clay. In: *Proceedings of the International Symposium on Soft Clay*, Asian Institute of Technology, 327–333.

[59] Zdravkoviċ, L. & Potts, D.M. (2003). Numerical study of the effect of preloading on undrained bearing capacity, *International Journal of Geomechanics,* ASCE*,* 3, No. 1, 1-10.